



## Article

# Designing the Signal Quality Monitoring Algorithm Based on Chip Domain Observables for BDS B1C/B2a Signals under the Requirements of DFMC SBAS

Xiang Wang <sup>1,2</sup> , Xiaowei Cui <sup>1,\*</sup>, Gang Liu <sup>1</sup> and Mingquan Lu <sup>1,3</sup><sup>1</sup> Department of Electronic Engineering, Tsinghua University, Beijing 100084, China<sup>2</sup> State Key Laboratory of Geo-Information Engineering, Xi'an 710054, China<sup>3</sup> Beijing National Research Center for Information Science and Technology, Tsinghua University, Beijing 100084, China

\* Correspondence: cxw2005@tsinghua.edu.cn

**Abstract:** To guarantee the integrity of a global navigation satellite system (GNSS) for safety-critical users, a satellite-based augmentation system (SBAS) makes use of the integrity monitoring architecture, of which the signal quality monitor (SQM) is an important component to address the potential risks caused by satellite-induced signal anomalies. Due to the introduction of dual-frequency multi-constellation (DFMC) techniques in 2025, the ranging uncertainty will be reduced by the elimination of first-order ionospheric delay, but the biases measured in each individual signal will be inflated by the ionosphere-free combinations. Moreover, multiple modulations of DFMC signals might introduce applicability uncertainty of a traditional SQM method that has been protecting GPS L1C/A signal only. Thus, higher requirements are put forward for future SQM methods in detection sensitivity and modulation independence. This paper first proposes a design methodology for the SQM algorithm for BDS B1C/B2a signals, which could be easily extended to the DF combinations of other GNSS core constellations. Then, by comparing the performances of SQM baseline algorithms based on traditional multi-correlator and emerging chip domain observables (CDOs), respectively, the superiority of CDO-based SQM is declared. Detailed design iterations are further discussed, including the algorithm practicalization with optimizing code-phase bin length and lowering sampling frequency, as well as the metric simplification, to promote the overall performance while preserving a lower implementation complexity. Ultimately, a CDO-based SQM algorithm for BDS B1C/B2a signals is reached, which would be considered as an effective candidate in new generation DFMC SBASs.

**Keywords:** satellite-based augmentation system (SBAS); BeiDou navigation satellite system (BDS); BeiDou satellite-based augmentation system (BDSBAS); signal quality monitor (SQM); dual-frequency multi-constellation (DFMC); chip domain observable (CDO); integrity



**Citation:** Wang, X.; Cui, X.; Liu, G.; Lu, M. Designing the Signal Quality Monitoring Algorithm Based on Chip Domain Observables for BDS B1C/B2a Signals under the Requirements of DFMC SBAS. *Remote Sens.* **2023**, *15*, 1008. <https://doi.org/10.3390/rs15041008>

Academic Editors:  
Damian Wierzbicki and  
Kamil Krasuski

Received: 16 December 2022

Revised: 10 February 2023

Accepted: 10 February 2023

Published: 12 February 2023



**Copyright:** © 2023 by the authors. Licensee MDPI, Basel, Switzerland. This article is an open access article distributed under the terms and conditions of the Creative Commons Attribution (CC BY) license (<https://creativecommons.org/licenses/by/4.0/>).

## 1. Introduction

The integrity of global navigation satellite systems (GNSSs), e.g., GPS, GLONASS, Galileo, and BDS, is an important performance indicator to safety-critical users, such as civil aircrafts in approaches. If a GNSS constellation failed to provide the expected nominal service but the users were not notified in time, an incident of loss of integrity would occur. Conventionally, the open service performances of individual GNSS core constellations can hardly meet the requirements of International Civil Aviation Organization (ICAO) for approaches with vertical guidance (APV) [1]. In order to enhance GNSS integrity for civil aviation users, several kinds of augmentation systems have been developed, one of which is called a satellite-based augmentation system (SBAS) that is intended to serve civil aviation in Category-I (CAT-I) precision approaches (PAs) [2]. Several SBASs have been operational for years, such as the wide-area augmentation system (WAAS) covering North America and the European geostationary navigation overlay service (EGNOS) covering Europe

and North Africa [3], etc. The BeiDou satellite-based augmentation system (BDSBAS) for China and its surrounding areas is under development and certification [3,4]. An SBAS applies geostationary earth orbit satellites (GEOs) to broadcast wide-area differential (WAD) corrections to promote GNSS positioning accuracy and ranging signals to improve GNSS geometries, hence, creating continuity and availability [2]. In addition, SBAS performs fault monitoring to provide integrity messages, as well as confidence of the WAD corrections for users, hence, to enhance GNSS integrity [5].

Signal quality monitoring (SQM), as a component of the integrity monitoring architecture of SBAS, was developed to protect users against potential distortions in GNSS signals caused by unexpected failures onboard satellites, of which the first observed occurrence is the GPS SVN-19 event [6]. The considered signal distortions, or so-called evil waveforms (EWFs), would manifest themselves differently in the receivers with different configurations, including the discriminator type of the tracking loop, the correlator spacing, and properties of the pre-correlation filter such as the 3-dB bandwidth, differential group delay, and roll-off rate out of band [7]. ICAO specifies a fixed configuration for SBAS reference receivers and a configuration space for user receivers due to the diversity of airborne receiver manufacturers. As a consequence, the configuration of avionics of an SBAS user may easily be different with that of the reference receiver, and, hence, a potential differential ranging bias caused by an EWF would be induced, invalidating the WAD corrections of SBAS. Reference [8] summarizes the observed EWF events of GPS till 2017, while Reference [9] introduces the evolution of SQM since WAAS was commissioned in 2003, indicating that SQM is still important to the integrity protection of SBASs, especially for those under development, e.g., BDSBAS.

The SQM algorithm is operated in three independent monitors at each individual reference station to measure the values of pre-defined metrics with the visible GNSS signals in real-time. Subsequently, the master station gathers and processes the reference SQM information and, hence, identifies whether any monitored signal(s) were anomalous [6]. Metric definition is critical to the performance of an SQM algorithm [7]. The metrics based on pseudorange observables are intuitively effective. However, it is complicated and budget consuming to measure and check the consistency among massive pseudoranges of a particular signal, with massive receivers traversing the given avionic configuration space at an individual station [6]. Since the cross-correlation function between an incoming anomalous signal and the local replica would be distorted, the current SQM metrics are generally based on multi-correlator observables (MCOs) that are conventionally pairs of Early (E) and Late (L) correlator values measured at different advances and latencies symmetrically of the correlation function. MCO-based metrics can be defined as utilizing all the measured correlator values to check the overall shape of the correlation function, e.g., alpha-metric in WAAS [10], or particular correlator values to check the slopes and/or symmetries of it, e.g., delta-metric and ratio-metric of SQM2b algorithm in EGNOS [11]. SQMs applying MCO-based metrics have been performing well in operational SBASs.

At present, all the operational SBASs are augmenting a single-frequency (SF) signal, i.e., GPS L1 C/A signal [3]. In 2025, technology of dual-frequency multi-constellation (DFMC) will be introduced to the next generation of SBAS [1], which is under standardization. Dual-frequency (DF) combination is able to eliminate first-order ionospheric delay, thus promote ranging accuracy, and a multi-constellation (MC) solution can improve the geometry of visible satellites, hence, GNSS continuity and availability. However, the required error limit of DF ranging will be much lower compared to that of SF ranging, while conversely, the errors will be amplified by 2.26 and 1.26 times for L1 and L5 frequencies by the ionosphere-free (iono-free) combinations, respectively [12]. As a consequence, the ICAO integrity criteria will have much higher requirements on SQM performance. On the other hand, DFMC signals with diversified modulation characteristics will be introduced to SQM, indicating that the potential distortions might manifest themselves differently in the correlation functions with different shapes. Therefore, a novel SQM method which is less modulation-dependent is expected. By focusing on the potentially anomalous signal itself,

a class of SQM methods based on chip domain observables (CDOs) is emerging. The chip-based outputs mainly have two benefits: the first is that the potential deformations would not be averaged down by the correlation process, hence, the detections might be more sensitive; while the second is that the CDOs are less dependent on the code modulations of interest, thus any detection method that acts on the code chip transitions of traditionally binary phase shift keying (BPSK) modulated signal could be adapted to other emerging modulations, such as binary offset carrier (BOC) [7,13].

The concept of CDO was first applied in the field of signal visualization. The development of the NovAtel Vision Correlator enables measurements in chip rising edges to visualize chip-shapes in hardware [14]. Reference [15] explained the mechanism of Vision technology and proposed a signal compression method to generalize the approaches of the Vision technology from a GPS L1 C/A signal to other GNSS signals. Moreover, Reference [16] presents a GPU-based chip-shape correlator architecture design with the implementation of signal compression to obtain high-resolution chip waveforms and cross-correlation functions, providing foundations for CDO-based applications with great flexibility. Based on high-gain parabolic dish antennas, References [17–19] promoted research on signal visualization, including computations of CDOs and the assessment of signal quality consistencies, etc. While in the field of SQM, the CDO-based SQM has been implemented in NovAtel G-III receivers with fixed configurations for WAAS [9], and the sensitivity and applicability compared to MCO-based ones was proved [13], but the algorithm design is inaccessible. Reference [20] proposed a CDO-based SQM algorithm also with fixed configurations and presented the superiority of a BDS B1C signal, while it was still lacking systematism. As systematic research, Reference [7] proposed a complete and generic design methodology for CDO-based SQM methods on the basis of derivation, simulation, and simplification, but it is generalized for BPSK(1)-, BOC(1,1)-, and BPSK(10)-modulated signals by utilizing three representative signals, ignoring the specificities in each individual GNSS core constellation and its DF signals. Nevertheless, the methodology proposed in Reference [7] is worthy to be applied in this paper. BDS-III has been providing global service since 2020. While in the same year, BDS B1C/B2a signals passed the full set of technical verification of ICAO and will be authorized to provide service for global avionics. Additionally, BDSBAS is under construction and the initial operational capability has been formed by 2022 [3]. Since the integrity is the prime concern of BDS performance and the prior factor of BDSBAS design for civil aviation users [21,22], the SQM of BDS B1C/B2a DF civil signals should be systematically studied. This paper (1) proposes a generic design methodology for an SQM algorithm, which can easily be extended to other DF combinations of GNSS core constellations, in the name of DFMC; (2) fully evaluates and analyzes the traditional MCO-based and the emerging CDO-based SQM baseline algorithms; and (3) derives a CDO-based algorithm for BDS B1C/B2a signals with the optimization of code-phase bin length, the practicalization of lowering sampling frequency, and the simplification of detection metrics, in order to promote overall performance, while preserving a lower implementation complexity. The rest of this paper is organized as follows: Section 2 introduces the contexts of BDS B1C/B2a signals and the fundamentals of SQM, Section 3 proposes the design methodology of an SQM algorithm as the core and direction of the whole paper, Section 4 details the discussions and derivations of the suggested algorithm, and Section 5 concludes the paper and envisions some future work as well.

## 2. Context of This Study

In order to clarify the main objectives of this article, some background is introduced in this section, including the characteristics of BDS B1C/B2a signals and the modeling of their risky deformations, as well as the basic concept of SQM and the observables to be applied of interest.

### 2.1. Structures and Modulation Characteristics of BDS B1C and B2a Signals

The DF civilian signals of BDS, i.e., B1C and B2a signals, are designated to be augmented by DFMC SBASs, and used for iono-free combinations in positioning solutions of civil aviation [23].

The complex envelope of the B1C signal is composed of the data component  $s_{B1C\_data}(t)$  and the pilot component  $s_{B1C\_pilot}(t)$ , between which the power ratio is 1:3. Moreover, the pilot component  $s_{B1C\_pilot}(t)$  is modulated by a QMBOC(6,1,4/33) composite subcarrier that is composed of BOC(1,1) and BOC(6,1) subcarriers with quadrature phases, between which the power ratio is 29:4 [24,25]. The expression of the B1C signal is given by:

$$\begin{aligned} s_{B1C}(t) &= s_{B1C\_data}(t) + j \cdot s_{B1C\_pilot}(t) \\ &= \sqrt{\frac{11}{44}} \cdot D_{B1C\_data}(t) \cdot C_{B1C\_data}(t) \cdot \text{sign}(\sin(2\pi f_{sc\_B1C\_a}t)) \\ &\quad + \sqrt{\frac{4}{44}} \cdot C_{B1C\_pilot}(t) \cdot \text{sign}(\sin(2\pi f_{sc\_B1C\_b}t)) + j \cdot \sqrt{\frac{29}{44}} \cdot C_{B1C\_pilot}(t) \cdot \text{sign}(\sin(2\pi f_{sc\_B1C\_a}t)) \end{aligned} \quad (1)$$

where  $D_{B1C\_data}$  is the navigation data,  $C_{B1C\_data/pilot}$  are the pseudo random noise (PRN) codes for data and pilot components, respectively, and  $f_{sc\_B1C\_a/b}$  are the frequencies of BOC(1,1) and BOC(6,1) subcarriers, i.e., 1.023 and 6.138 MHz, respectively.

Similarly, the complex envelope of the B2a signal consists of the BPSK(10)-modulated data component  $s_{B2a\_data}(t)$  and pilot component  $s_{B2a\_pilot}(t)$  as well, between which the power ratio is 1:1 [24,26]. The expression of the B2a signal is given by:

$$s_{B2a}(t) = s_{B2a\_data}(t) + j \cdot s_{B2a\_pilot}(t) = \sqrt{\frac{1}{2}} \cdot D_{B2a\_data}(t) \cdot C_{B2a\_data}(t) + \sqrt{\frac{1}{2}} \cdot C_{B2a\_pilot}(t) \quad (2)$$

where  $D_{B2a\_data}$  is the navigation data, and  $C_{B2a\_data/pilot}$  are the PRN codes for data and pilot components, respectively.

A DF receiver shall use a BOC(1,1) replica for B1C pilot signal and BPSK(10) replica for B2a pilot signal for iono-free combination [23]. The signal structures and modulation characteristics are listed in Table 1.

**Table 1.** The structures and modulation characteristics of BDS B1C and B2a signals.

Signal	Signal Components	Center Frequency (MHz)	Modulation	Phase	Power Ratio	Symbol Rate (sps)
BDS B1C	data	$s_{B1C\_data}(t)$	BOC(1,1)	0	11/44	100
	pilot	$s_{B1C\_pilot\_a}(t)$	QMBOC	90	29/44	0
		$s_{B1C\_pilot\_b}(t)$	(6,1,4/33)	BOC(6,1)	0	
BDS B2a	data	$s_{B2a\_data}(t)$	BPSK(10)	0	1/2	200
	pilot	$s_{B2a\_pilot}(t)$		90	1/2	0

### 2.2. Threat Models and Threat Spaces of BDS B1C and B2a Signals

ICAO adopts a 2nd-order step (2OS) model as a standard threat model (TM) [1]. The 2OS-TM is defined in code signals. The signal generation hardware onboard a satellite is considered as a cascade of digital and analog components [6], thus, the EWFs caused by the hardware failures are classified into digital distortion (TM-A), analog distortion (TM-B), and combined distortion (TM-C):

- TM-A accounts for the non-ideal characteristics in the consistency of the chip period and is modeled as an advance or delay of chip falling edges. A parameter  $\Delta$  in chips is used to represent this bias.
- TM-B takes the non-ideal characteristics in the amplitude modulations of rectangular waves into consideration and is modeled as the damped oscillations after chip transitions. Two parameters, i.e., the damped frequency of oscillation  $f_d$  in mega-hertz

(MHz) and the damping factor  $\sigma$  in mega-neper per second (MNp/s), are used. The damped oscillation is expressed by:

$$e(t) = \begin{cases} 0 & t < 0 \\ 1 - e^{-\sigma t} \cdot \left( \cos 2\pi f_d t + \frac{\sigma}{2\pi f_d} \cdot \sin 2\pi f_d t \right) & t \geq 0 \end{cases} \quad (3)$$

- TM-C is the simultaneous occurrence of TM-A and TM-B.

Given the TM of a particular signal, all the possible EWFs that may induce larger differential errors are included in the threat space (TS). The TS should be sufficient and necessary, and any other EWFs outside the TS need not be considered in that the ranging errors they might induce are small enough to be ignored or large enough to be perceived by the onboard monitors [22] and/or reference receivers, or the corresponding EWF parameters are physically impossible either [6].

Due to the similarity in the composition of signal generation hardware onboard, as well as the simplicity and maturity of the 2OS-TM, the TMs of B1C and B2a signals are proposed in the form of the 2OS-TM [27]. In addition, the TSs of B1C and B2a signals are also tested and proposed to ICAO [27], which will be adopted in the next edition of ICAO standards and recommended practices (SARPs). Table 2 lists the TSs of B1C and B2a signals in the form of EWF parameter value ranges.

**Table 2.** The threat spaces of BDS B1C and B2a signals.

Signal	Threat Model	$\Delta$ (Chips)	$f_d$ (MHz)	$\sigma$ (MNp/s)
BDS B1C	TM-A	−0.05+0.05	—	—
	TM-B	—	1.5–18	0.1–20
	TM-C	−0.05+0.05	1.5–18	0.1–20
BDS B2a	TM-A	−0.5+0.5	—	—
	TM-B	—	4–18	0.1–18
	TM-C	−0.5+0.5	4–18	0.1–18

### 2.3. Performance Indicators of SQM

SQM detects potential EWFs in the monitored signals to protect users against hazardous misleading information (HMI) caused by onboard failures. Thus, it provides a connection between the signal domain where detections are actually carried out and the ranging domain where pseudoranges are measured [7].

SQM measures the values of pre-defined metrics with a monitored signal and compares them with their nominal values against corresponding thresholds, as which the values of minimum detectable errors (MDEs) are applied in detections. The expression of the  $j$ -th MDE is given by [1]:

$$\text{MDE}_j = (K_{\text{ffd}} + K_{\text{md}}) \cdot \sigma_j \quad (4)$$

where  $\sigma_j$  is the nominal standard deviation of the  $j$ -th metric value, and  $K_{\text{ffd}} \approx 5.26$  and  $K_{\text{md}} \approx 3.09$  are the Gaussian quantiles corresponding to the required probabilities of fault-free detection ( $1.5 \times 10^{-7}$  per test) and miss detection ( $1 \times 10^{-3}$  per test) for CAT-I PA of civil aviation, respectively [1]. Generally speaking, MDEs are the amount of distortions that are required to guarantee a given SQM test [6]. In other words, an MDE provides the largest scale for variations of the nominal value of a metric, covering risks of continuity and integrity at the same time for conservativeness.

In the ranging domain, the tolerable errors are delimited by the maximum error range residuals (MERRs), which are assumed as the maximum differential pseudorange error (maxPRE) with the worst GNSS geometry, but without producing HMI [6]. For SF differential ranging, MERR is expressed by [1]:

$$\text{MERR}_{\text{SF}} = K_{\text{V,PA}} \cdot \sqrt{\sigma_{i,\text{UDRE}}^2 + \min\{\sigma_{i,\text{UIRE}}^2\}} \quad (5)$$

where  $K_{V,PA} \approx 5.33$  is the Gaussian quantile for the vertical direction of PA and APV modes, and  $\sigma_{i,UDRE}$  and  $\sigma_{i,UIRE}$  are the standard deviations of user differential ranging error (UDRE) and user ionospheric ranging error (UIRE) of the  $i$ -th satellite, respectively. For DF avionics using L1/L5 iono-free combinations, 1st-order ionospheric delay will be eliminated, hence MERR becomes:

$$\text{MERR}_{DF} = 5.33 \cdot \sigma_{i,DFRE} \quad (6)$$

where  $\sigma_{i,DFRE}$  is the standard deviations of dual-frequency ranging error (DFRE) of the  $i$ -th satellite. UDRE index (UDREI) is a broadcast indicator defining  $\sigma_{UDRE}$  [1]. Reference [28] stated the minimum MERR of 6.1 m indicates the operational minimum UDREI of 4, while Reference [10] showed the  $\sigma_{UDRE}$  floor for L1-only WAAS of 0.75 m that corresponds to a virtual non-integer UDREI between 4 and 5 as the smallest UDRE the L1-only WAAS can provide. With accordance to the relation between UDREs and UDREIs in Reference [13], the MERR for SF differential ranging is given by:

$$\text{MERR}_{SF} = 6.08 \text{ m} \quad (7)$$

as having been applied for decades. Naturally, the DFRE index (DFREI) of 4 will be used for DF ranging, and  $\text{UDRE}_4 = 2.25 \text{ m}$  will also be extended to  $\text{DFRE}_4 = 2.25 \text{ m}$ . Given the required availability of 99.9% [29], the relationship between DFRE and  $\sigma_{DFRE}$  is  $\text{DFRE} = 3.29 \cdot \sigma_{DFRE}$ . Thus, the value of  $\text{MERR}_{DF}$  is given by:

$$\text{MERR}_{DF} = 3.64 \text{ m} \quad (8)$$

with a combination of Equation (6). However, the biases in the individual SF signals of the iono-free combination would be inflated, as expressed by:

$$\rho_{DF} = 2.26 \cdot \rho_{L1} - 1.26 \cdot \rho_{L5} \quad (9)$$

Thus, to guarantee safety, the following inequality should be met:

$$2.26^2 \cdot b_{L1}^2 + 1.26^2 \cdot b_{L5}^2 \leq 3.64^2 \quad (10)$$

where  $b_{L1}$  and  $b_{L5}$  are the biases in the individual SF signals, respectively.

The definition of MDE in Equation (4), the values of MERR in Equation (8), and the constraint to pseudorange biases in Equation (10) will be applied in later discussions.

#### 2.4. Basis of MCO-Based vs. CDO-Based SQMs

An SQM algorithm applies observables to construct detection metrics, including pseudorange observables, multi-correlator observables (MCOs), and chip domain observables (CDOs), as introduced above. Traditional MCO-based SQM algorithms have been operational for decades, providing satisfactory protection for GPS L1C/A signals in SF SBASs. However, toward the needs and requirements of protection for DFMC signals, traditional SQM algorithms are facing significant challenges. This subsection gives a comparison between the traditional and emerging SQM algorithms in terms of basic observables, i.e., MCO vs. CDO.

Correlation function is critical to GNSS signal acquisition and tracking. Since an EWF might distort the cross-correlation function (CCF) between an incoming signal and its local replica in a receiver, the technique of multi-correlation was developed [6]. Given the incoming signal  $s(t)$  and its local replica  $p(t)$ , the CCF is given by:

$$R(\tau) = \int_0^{T_{corr}} s(t)p(t - \tau)dt \quad (11)$$

where  $T_{corr}$  is the correlation period. For a conventional tracking loop with an E-L discriminator, three correlators are used, i.e., Early (E), Prompt (P), and Late (L), and the

corresponding in-phase components of correlator values are expressed as  $I_E$ ,  $I_P$ , and  $I_L$ , respectively. If multiple offsets are applied to densify the conventional three correlators, multiple correlator values that are slaved to the E-L tracking pair [1] will be measured to obtain the discretized shape of the correlation function. For example, a scheme of 9 correlators distributed between  $-0.10$  and  $+0.10$  chips with  $0.025$ -chip spacings is provided in Reference [1]. Provided the conditions that the tracking loop has been locked and the carrier wipeoff process performed, the MCOs refer to all the in-phase components of the multi-correlator values.

As introduced, DFMC technology will put forward more stringent requirements on SQMs, i.e., the error-inflating effect induced by DF iono-free combination against the tightened MERR limit, as well as the differences of deformation magnitudes in CCFs affected by the different chip rates and modulations of DFMC signals. Since the 2OS-TM is defined in code signal, CDO-based SQM methods are emerging. Similarly, provided the conditions that the tracking loop has been locked and the carrier wipeoff process performed, each individual chip is segmented into  $M$  bins with equal length conventionally, hence,  $M$  raw CDOs are obtained. Furthermore, the raw CDOs are normalized by  $I_P$  to eliminate the impact of navigation bits on the signs [7]. Then, the  $i$ -th normalized CDO is given by:

$$\text{CDO}_{i,nml} = \frac{1}{I_P} \cdot \frac{1}{N_{\text{bin}_i}^{\text{samp}}} \cdot \sum_{j=1}^{N_{\text{bin}_i}^{\text{samp}}} \text{SP}(j) \quad (12)$$

where  $N_{\text{bin}_i}^{\text{samp}}$  is the number of digitized sample points collected by  $\text{bin}_i$  within the specified integration period  $T_{\text{int}}$ , and  $\text{SP}(j)$  is the value of the  $j$ -th sample. A normalized CDO is physically an averaged and normalized measurement of the digitized samples within  $T_{\text{int}}$ , thus  $M$  normalized CDOs are consecutively output with the period of  $T_{\text{int}}$ .

CDOs are measured when the tracking loop has been fixed by the E-L discriminator, indicating that the implementation complexity of CDO measurements is higher than the traditional E-P-L tracking loop with 3 correlators. While for the tracking loop with multi-correlators, the situation might be changed. On the one hand, CDO measurements have lower incremental complexity than MCO measurements do [19]. Theoretically, for a tracking loop with multi-correlators, a pair of complete multiplication and accumulation operations of correlation process are required if the MCOs of one more E-L correlator pair are needed to output. On the contrary, if an additional CDO is needed to output, only the code-phase bin length should be reassigned, and an accumulator added. On the other hand, modern receivers have become multi-functional with the development of hardware and software. In fact, a software-defined-radio (SDR) receiver equipped with GPU can achieve high definition measurements of CCF (at least 39 correlators) and chip transition of DFMC signals by applying the technique of chip-shape correlation in real time, the performance of which is comparable to that of a traditional multi-correlator technique with only 5 correlators [16]. Therefore, the hybrid SQM method proposed in Reference [30], where BDS B1C and B2a signals apply CDO- and MCO-based SQM algorithms, respectively, is far from optimal.

### 3. Design Methodology of SQM Algorithm

SQM design is a complicated and systematic job, where several sophisticated elements are involved, as indicated in Section 2, including: (1) the TM with configurable parameters in a physically credible TS to cover the diversified EWFs that are potentially generated by the satellites to cause hazardous differential ranging errors; (2) the specified user receiver configuration space (URCS) with all the aspects taken into account that might affect the ranging error of a signal; (3) the specially defined metrics with enough sensitivities to reflect the differences between a deformed and the nominal signals. On the other hand, the performance of an SQM algorithm is reflected by the correspondence between the signal

and the ranging domains, which is extremely uncertain due to the sophisticated elements above, because:

- fundamentally, the expressions of the 2OS-TM and the filtering effect make any one particular point in the deformed chip waveforms or correlation peak have the form of transcendental function;
- further in the signal domain, the diversity of the specified TS and the defined metrics make it impossible to abstract the tens of thousands of detection results into closed-form formulae;
- and in the ranging domain, the diversity of the specified TS and the broadness of the required URCS make it impossible to obtain a closed-form expression for the maxPREs.

Thus, the design and evaluation of an SQM algorithm is conventionally performed based on massive simulations, such as the SQM2b algorithm [6] that was applied in EGNOS [11] and the  $\alpha$ -metric applied in the legacy WAAS [10].

More specifically, for an MCO-based SQM algorithm, although the integral expressions of a distorted CCF have been derived in Reference [6], the analytical solutions in the ranging domain are hard to reach. While for a CDO-based SQM algorithm, Reference [7] draws ten influential factors out of the operations, of which the code-phase bin length, BIN, and the sampling frequency,  $F_S$ , are the most important. Different values of BIN may force each code-phase bin to incorporate samples differently in calculating a CDO value, while different values of  $F_S$  will allow different quantities of samples to be incorporated thoroughly. However, it is still difficult to give either a closed-form formula for calculating a CDO value or an analytical ranging bias with the CCF, in the signal or the ranging domains, respectively. Therefore, the design and evaluation of an SQM algorithm for BDS B1C and B2a signals in this paper is based on massive simulations as well. Figure 1 shows the design methodology of the SQM algorithm for BDS B1C and B2a signals.

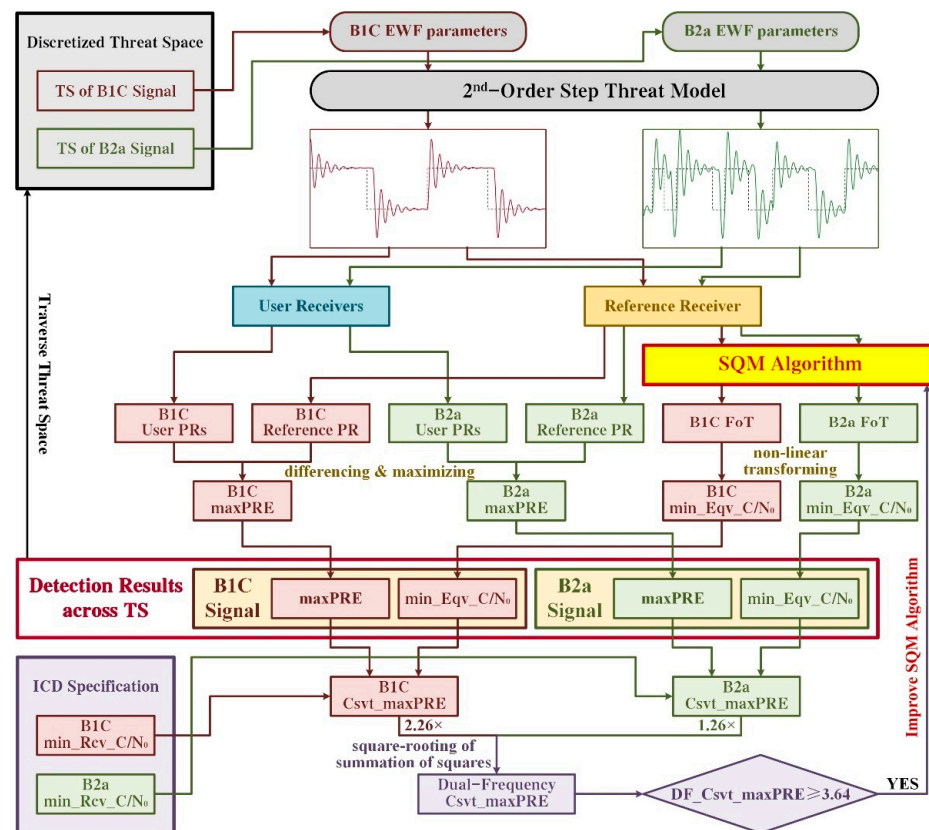


Figure 1. Design methodology of SQM algorithm for BDS B1C and B2a signals.

The SQM algorithm design for BDS B1C and B2a signals operates as follows:

(1) The TS of B1C/B2a signal is discretized into tens of thousands of threat points, each of which consists of three EWF parameters. The discretization applied in this paper is given in Table 3.

**Table 3.** Discretization of the threat spaces of BDS B1C and B2a signals.

Signal	Threat Model	$\Delta$ (Chips)	$f_d$ (MHz)	$\sigma$ (MNp/s)
BDS B1C	TM-A	−0.05:0.01:−0.01, +0.01:0.01:+0.05	—	—
	TM-B	—	1.5:0.5:18	0.1, 0.5:0.5:20
	TM-C	−0.05:0.01:−0.01, +0.01:0.01:+0.05	1.5:0.5:18	0.1, 0.5:0.5:20
BDS B2a	TM-A	−0.5:0.1:−0.1, +0.1:0.1:+0.5	—	—
	TM-B	—	4:0.5:18	0.1, 0.5:0.5:18
	TM-C	−0.5:0.1:−0.1, +0.1:0.1:+0.5	4:0.5:18	0.1, 0.5:0.5:18

(2) Draw a threat point out of the discretized TS of B1C/B2a signal to generate the corresponding EWF by applying the 2OS-TM. The formulation of EWF-generation is based on the simulative method in Reference [31]. As examples in Figure 1, the EWF of B1C in red is generated with  $\Delta = 0.05$  chips,  $f_d = 15$  MHz, and  $\sigma = 11$  MNp/s, and that of B2a in green is with  $\Delta = 0.5$  chips,  $f_d = 15$  MHz, and  $\sigma = 11$  MNp/s. Note that the chip period of B1C signal is ten times that of the B2a signal. The black dashed lines represent the corresponding ideal rectangle waveforms, respectively.

(3) The generated EWF of the B1C/B2a signal is processed by the reference receiver and numerous user receivers. The specified receiver configurations given in Table 4 are consistent with the specifications in Reference [23]. Each receiver will measure a bias that is caused by the combination of signal deformation and receiver configuration. This bias is denoted as PR in Figure 1 to represent a measured pseudorange only with differential-mode errors. The absolute difference between the Reference PR and a User PR seems to be the differential pseudo-range error experienced by this particular user. By performing this differencing process between the Reference PR and tens of User PRs, the maximum one of the tens of calculated differential pseudorange errors is the maxPRE of the threat point. The calculated maxPRE of the B1C/B2a signal should be saved in Detection Results.

**Table 4.** Configurations of reference and user receivers.

Receiver	Reference		User	
	BDS B1C	BDS B2a	BDS B1C	BDS B2a
Tracking	E-L BOC(1,1) local replica	E-L BPSK(10) local replica	E-L BOC(1,1) local replica	E-L BPSK(10) local replica
Correlator Spacing (chips)	0.10	1.0	0.08, 0.10, 0.12	0.9, 1.0, 1.1
Pre-correlation Bandwidth (double-sided, MHz)	24		12, 14, 16, 18, 20, 22, 24	

Table 4. Cont.

Receiver	Reference		User	
Signal	BDS B1C	BDS B2a	BDS B1C	BDS B2a
Filter	6th-order Butterworth		(1) 6th-order Butterworth (2) mixed Butterworth <sup>1</sup> (3–6) four types of resonators <sup>2</sup>	

<sup>1</sup> The mixed Butterworth filter has the same amplitude response as 6th-order Butterworth and 0 nanoseconds differential group delay. <sup>2</sup> The four types of resonator filters are with 24/30 dB per octave gain roll-off and 0/150 nanoseconds differential group delay, respectively.

(4) The reference receiver will also send the generated EWF of B1C/B2a signal to a designed SQM algorithm in the bright yellow rectangle in Figure 1. The SQM algorithm will measure values of the defined metrics with the EWF, and then compare the measured metric values to their nominal ones against corresponding MDEs. The maximum one of the calculated ratios is designated as the figure of test (FoT) of the SQM algorithm to this threat point. The obtention of an FoT value is given by:

$$\text{FoT} = \max_{1 \leq j \leq N} \left\{ \frac{|\text{metric}_j^{\text{EWF}} - \text{metric}_j^{\text{nom}}|}{\text{MDE}_j} \right\} \quad (13)$$

where  $N$  represents the number of defined metrics and the superscript nom is the abbreviation for nominal. The FoT value will be non-linearly transformed into a value of minimum equivalent carrier-to-noise ratio ( $\text{min\_Eqv\_C}/N_0$ ). The calculated values of  $\text{min\_Eqv\_C}/N_0$  for the B1C/B2a signal should be saved in Detection Results.

(5) Traverse the discretized TS of the B1C/B2a signal until the values of maxPRE and  $\text{min\_Eqv\_C}/N_0$  of all the threat points are obtained.

(6) Calculate the values of minimum receiving carrier-to-noise ratio ( $\text{min\_Rcv\_C}/N_0$ ) of the B1C and B2a signals in accordance with the corresponding interface control documents (ICDs) [25,26] for conservativeness, given by:

$$\begin{cases} \text{B1C} : -161 \text{ dBW} + 10 \cdot \log_{10}(29/44) - 0.3 \text{ dB} - 5.5 \text{ dB} - (-228.6 \text{ dBJ/K} + 24.8 \text{ dBK}) = 35.2 \text{ dB-Hz} \\ \text{B2a} : -158 \text{ dBW} + 10 \cdot \log_{10}(1/2) - 0.6 \text{ dB} - 5.5 \text{ dB} - (-228.6 \text{ dBJ/K} + 24.8 \text{ dBK}) = 36.7 \text{ dB-Hz} \end{cases} \quad (14)$$

where  $-161 \text{ dBW}$  and  $-158 \text{ dBW}$  are the minimum received power levels on ground,  $-0.3 \text{ dB}$  and  $-0.6 \text{ dB}$  are the correlation losses,  $-5.5 \text{ dB}$  is more conservative [1,27] than the  $-3.1\text{-dB}$  antenna gain of the omnidirectional NovAtel GNSS-750 antenna at 5-degree elevation [32], and  $-228.6 \text{ dBJ/K}$  and  $24.8 \text{ dBK}$  are calculated with the Boltzmann constant and the operating temperature of 300 K, respectively. In addition, the operation of 100-s metric-smoothing is conventionally applied to smooth down the poorly spatially- and/or temporally-correlated code noise and multipath errors, from which a smoothing gain no lower than 4 dB is expected [11]. Thus, the values of  $\text{min\_Rcv\_C}/N_0$  of B1C and B2a signals for the design and evaluation of SQM algorithm in this paper are set to 39.2 and 40.7 dB-Hz, respectively. Note that the GEOs and inclined geosynchronous orbit satellites (IGSOs) of BDS are invisible to some other important DFMC SBASs that will be monitoring BDS signals, e.g., WAAS and EGNOS, but only medium Earth orbit satellites (MEOs). Thus, the values would be 2 dB higher for both signals [25,26]. However, for conservative discussions, the values of IGSOs are applied for generality.

(7) The detection result of the B1C/B2a signal consists of a group of maxPRE values and a group of  $\text{min\_Eqv\_C}/N_0$  values that are corresponding to the discretized TS. Consequently, the monotonically descending confidence bounds provided by the tested SQM algorithm will be obtained with ascending carrier-to-noise ratio values ( $C/N_0$ ) to overbound the corresponding maxPRE values. Thus, given the  $\text{min\_Rcv\_C}/N_0$  of the B1C/B2a signal, the value of conservative maxPRE (Csvt\_maxPRE) will be found out.

(8) The errors in each of the individual SF signals will be inflated in the iono-free combinations in accordance with Equation (9). Thus, the  $C_{svt\_maxPRE}$ s of B1C and B2a signals need be multiplied by 2.26 and 1.26, respectively. Subsequently, calculate the summation of the squares of the inflated  $C_{svt\_maxPRE}$ s and then the square-root of it to reach the dual-frequency conservative maxPRE ( $DF\_C_{svt\_maxPRE}$ ).

(9) According to Equation (10), compare the calculated  $DF\_C_{svt\_maxPRE}$  with 3.64 m ( $DFREI = 4$ ). If the 3.64-m limit is exceeded, the tested SQM algorithm should be improved and the whole procedure shall be run again. Otherwise, the tested SQM algorithm is capable of protecting DF users against HMI induced by distorted signals, and the evaluation is accomplished.

Note that there is conventionally a reference-averaging process among the corresponding metric values from different in-view reference stations to a satellite to average down the differential-mode errors, such as thermal noise and local multipath, based on the fault-free hypothesis of satellite-free differential-mode errors. However, there exists significant uncertainties in the practical distributions and elevations of the visible stations to the same satellite. Besides, the satellite-induced elevation-dependent tracking errors ever observed in GPS SVN-49 and BDS-II signals might introduce the risks of reference-averaging invalidity [33]. Thus, it should be emphasized that the reference-averaging gain shall not be considered in SQM algorithm design.

In order to reduce implementation complexity, some simplifications and/or optimizations might be needed, including those by simplifying the hardware implementations or reducing the number of metrics while sustaining the expected detection capability.

#### 4. SQM Algorithm Design for BDS B1C and B2a Signals

The procedure of SQM algorithm design will be performed in this section in accordance with the design methodology proposed in Figure 1. Since MCO-based SQM methods are commonly used in L1-only SBASs, the MCO-based baseline algorithm proposed in Reference [11] is first applied to initialize design procedure. As the second iteration of the design procedure, a CDO-based algorithm with generally optimal configuration given in Reference [7] is evaluated, which seems to be the CDO-based baseline algorithm. In order to seek the genuine optimal code-phase bin length for BDS B1C/B2a combination while lowering the required sampling frequency for general implementation, the operations of practicalization including the optimizations of bin length and the iterations of algorithm evaluation are performed. With the practically optimal configuration, the sensitivity of CDO-based metrics is tested to reduce the number of metrics, accounting for the computational complexity while sustaining the expected performance in meeting the ICAO requirements for CAT-I PA.

##### 4.1. Evaluation of the MCO-Based SQM Baseline Algorithm

In order to achieve the baseline performance of the MCO-based SQM algorithm, we apply schemes with dense distributions of correlators, i.e.:

- for the B1C signal, 51 correlators are utilized, which are uniformly distributed between  $-0.25$  and  $+0.25$  chips with 0.01-chip spacings in the CCF;
- for the B2a signal, 21 correlators are utilized, which are uniformly distributed between  $-1.0$  and  $+1.0$  chips with 0.1-chip spacings in the CCF.

Moreover, the detection metrics are defined as:

$$\begin{cases} \text{metric}_{\text{simple-ratio}} \triangleq I_x / I_P \\ \text{metric}_{\text{diff-ratio}} \triangleq (I_{-x} - I_x) / I_P \\ \text{metric}_{\text{sum-ratio}} \triangleq (I_{-x} + I_x) / I_P \end{cases} \quad (15)$$

where  $I_x$  is the in-phase component of an E or L correlator value, and  $I_P$  is that of the P correlator value. Reference [11] states that this scheme would achieve particularly favorable SQM performance.

With the conditions of (1) the minimum received power levels on ground for BDS IGSOs; (2) the minimum receiving elevation of 5 degrees; and (3) the minimum 4-dB gain provided by the 100-s metric-smoothing operations, the considered conservative  $\min\_Rcv\_C/N_0$  values of B1C and B2a signals are 39.2 and 40.7 dB-Hz, respectively, as derived in Section 3. Note that the MDEs that are theoretically used as detection thresholds in SQM algorithm design are proportional to the standard deviations of nominal values of corresponding metrics, as indicated in Equation (4). For conservativeness, the above  $\min\_Rcv\_C/N_0$  values are selected as the worst nominal. The expressions of variations of the metrics defined in Equation (15) are given by:

$$\left\{ \begin{array}{l} \text{simple} : \left\{ \begin{array}{ll} \left( \frac{6|x| - 9|x|^2}{MK^2} - \frac{(1 - 3|x|)^2}{(MK^2)^2} \right) & \text{B1C}(-0.5 \leq x \leq +0.5) \\ \left( \frac{2|x| - |x|^2}{MK^2} - \frac{(1 - |x|)^2}{(MK^2)^2} \right) & \text{B2a}(-1.0 \leq x \leq +1.0) \end{array} \right. \\ \text{diff} : \left\{ \begin{array}{ll} 12|x|/MK^2 & \text{B1C}(-0.25 \leq x \leq +0.25) \\ 4|x|/MK^2 & \text{B2a}(-0.5 \leq x \leq +0.5) \\ 2/MK^2 & \text{B2a}(0.5 < |x| \leq 1.0) \end{array} \right. \\ \text{sum} : \left\{ \begin{array}{ll} \left( \frac{12|x| - 36|x|^2}{MK^2} - 4 \cdot \frac{(1 - 3|x|)^2}{(MK^2)^2} \right) & \text{B1C}(-0.25 \leq x \leq +0.25) \\ \left( \frac{4|x| - 4|x|^2}{MK^2} - 4 \cdot \frac{(1 - |x|)^2}{(MK^2)^2} \right) & \text{B2a}(-0.5 \leq x \leq +0.5) \\ \left( \frac{2 - 4 \cdot (1 - |x|)^2}{MK^2} - 4 \cdot \frac{(1 - 3|x|)^2}{(MK^2)^2} \right) & \text{B2a}(0.5 < |x| \leq 1.0) \end{array} \right. \end{array} \right. \quad (16)$$

where  $MK^2 = 2 \times 10^{(C/N_0)/10}$ . Note that the expressions for diff- and sum-ratio metrics with  $0.25 < |x| \leq 0.5$  for the B1C signal are not given due to the definition that the correlator values of interest are only distributed between  $-0.25$  and  $+0.25$  chips. By square-rooting the results in Equation (16), the standard deviations of MCO-based metrics with given  $C/N_0$  will be obtained for calculating corresponding MDEs. The derivations corresponding to Equation (16) are detailed in Appendix A.

Figure 2a,b show the evaluation results of the MCO-based SQM baseline algorithm for B1C and B2a signals, respectively, where the blue scatters represent the correspondence between the  $\min\_Eqv\_C/N_0$  and  $\maxPRE$  values of a threat point within the discretized TS, the green vertical dashed lines indicate the given  $\min\_Rcv\_C/N_0$  value of a signal, and the red horizontal lines give the corresponding  $Csvt\_maxPRE$  value of a signal guaranteed by the SQM algorithm. As shown in Figure 2, the  $DF\_Csvt\_maxPRE$  value of BDS B1C/B2a combinations guaranteed by the MCO-based SQM baseline algorithm is calculated as:

$$DF\_Csvt\_maxPRE_{MCO} = \sqrt{(2.00 \times 2.26)^2 + (0.21 \times 1.26)^2} \approx 4.53 > 3.64 \text{ m} \quad (17)$$

Therefore, the MCO-based SQM baseline algorithm can only provide a protection equivalent to  $DFREI = 5$  [13], not meeting the preset condition of  $DFREI=4$ . Since the baseline performance of MCO-based SQM is unsatisfactory, the emerging CDO-based methods will be tested.

#### 4.2. Evaluation of the CDO-Based SQM Baseline Algorithm

Reference [7] gives a generally optimal SQM algorithm based on CDOs for DFMC SBAS, called the SCSQM8r algorithm. The sampling frequency and the sectionalization of code-phase bins are the core influential factors of a CDO-based SQM algorithm [7]. In this subsection, an algorithm with a sampling frequency of 72 MHz and bins of 0.025 B1-chips is evaluated to find out the relatively more advantageous performance.

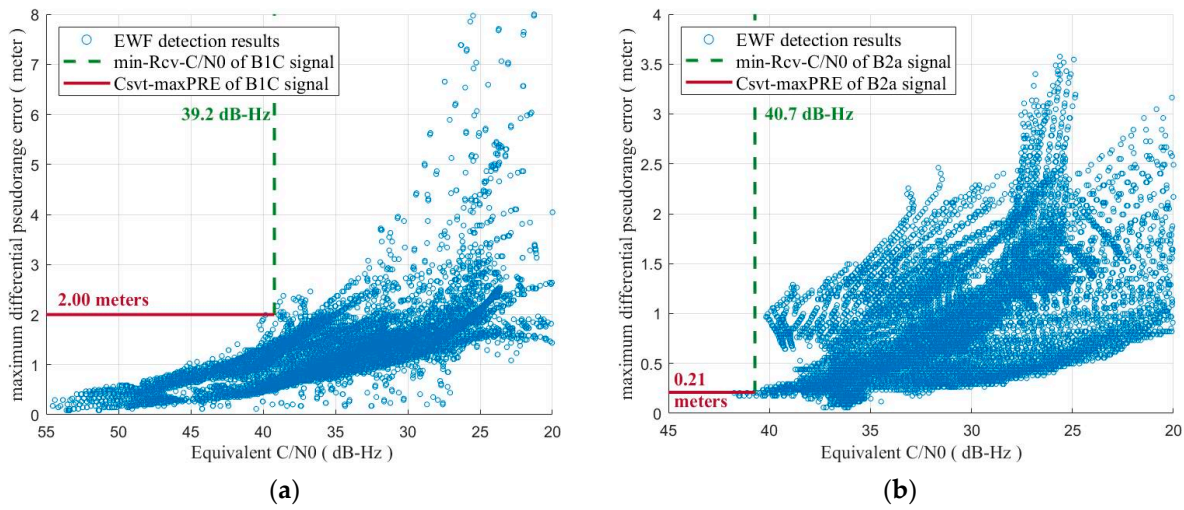


**Figure 2.** Evaluation results of the MCO-based SQM baseline algorithm. (a) B1C signal; (b) B2a signal.

The SCSQM8r algorithm applies 8 CDOs in the chip rising edges, which are denoted as  $CDO_1, CDO_2, \dots, CDO_8$  serially and distributed with 0.025 B1-chip spacings symmetrically. Moreover, the 8 CDOs are directly utilized as 8 metrics, aiming to achieve the primary performance of CDO-based SQM algorithm. In the CDO-based SQM baseline algorithm discussed in this subsection, the 8 CDOs are also applied but the metrics are expanded as:

$$\left\{ \begin{array}{l} \text{single-CDO : } \text{metric}_{\text{SCDO}} = CDO_i, 1 \leq i \leq 8 \\ \text{dual-CDO : } \text{metric}_{\text{DCDO}} = \frac{1}{2}(CDO_i \pm CDO_j), 1 \leq i \neq j \leq 8 \\ \text{triple-CDO : } \text{metric}_{\text{TCDO}} = \frac{1}{3}(CDO_i \pm CDO_j \pm CDO_k), 1 \leq i \neq j \neq k \leq 8 \\ \text{quad-CDO : } \text{metric}_{\text{QCDO}} = \frac{1}{4}(CDO_i \pm CDO_j \pm CDO_k \pm CDO_m), 1 \leq i \neq j \neq k \neq m \leq 8 \end{array} \right. \quad (18)$$

to hopefully achieve a better performance. Since the noise in a CDO is Gaussian [7], the powers and/or the products of CDOs are not applied as metrics due to the computational complexities in theoretical derivations and/or practical operations induced by the Chi-square distribution, and the quotients of CDOs are not applied either because of the inexistence of mean and variation of Cauchy variables. The numbers of single-, dual-, triple-, and quad-CDO metrics are given by:

$$\left\{ \begin{array}{l} \text{single-CDO : } 1 \times C_8^1 = 8 \\ \text{dual-CDO : } 2 \times C_8^2 = 56 \\ \text{triple-CDO : } 4 \times C_8^3 = 224 \\ \text{quad-CDO : } 8 \times C_8^4 = 560 \end{array} \right. \quad (19)$$

respectively. Therefore, the combinations of more than four CDOs are also not applied as metrics for the sake of computational complexity.

As indicated in Equation (12), a CDO is the mean of all the samples captured by the same bins of all the rising edges within a given integration period. The incorporated samples from the RF front-end output are deemed independent and identically distributed (IID) and affected by additive white Gaussian noise (AWGN) [17]. As a consequence, the standard deviation of a CDO is affected by the standard deviation of the AWGN and the number of samples incorporated. Since the fact that neither the sampling frequency could be divided exactly by the chip rate nor rising edges are uniformly distributed in the code sequences, 8 standard deviations of the corresponding 8 CDOs must be inconsistent but tend to be identical for a longer integration period [7]. The theoretical expression of the nominal standard deviation of a CDO is given in Reference [7] as

$$\sigma_{\text{CDO}} = \frac{BW}{I_P \cdot F_S \cdot \sqrt{2} \cdot T_{\text{int}} \cdot \text{RER} \cdot \text{BIN}} \cdot 10^{-\frac{C/N_0}{20}} \quad (20)$$

where  $BW$  is the double-sided pre-correlation bandwidth,  $F_S$  is the sampling frequency of the RF front-end output, RER is the abbreviation of rising edge rate that is a ratio from the quantity of rising edges to that of chips within one code period, and BIN is the proportion of a bin to a chip. The minimum value of  $I_P \cdot \sqrt{RER}$  across all the PRNs is applied for conservativeness, given in Reference [7]. The standard deviations of dual-, triple-, and quad-CDO metrics can be derived based on Equation (20).

Figure 3 shows the evaluation results of the CDO-based SQM baseline algorithm with a sampling frequency of 72 MHz and bins of 0.025 B1-chips for B1C and B2a signals, respectively, where the performances are superior to those in Figure 2. The resulted DF\_Csvt\_maxPRE is 0 m, indicating that a protection equivalent to DFREI = 0 [13] could be provided. Note that the performances in Figure 3 are also better than those given in Reference [7] due to the application of additional dual-, triple-, and quad-CDO metrics.

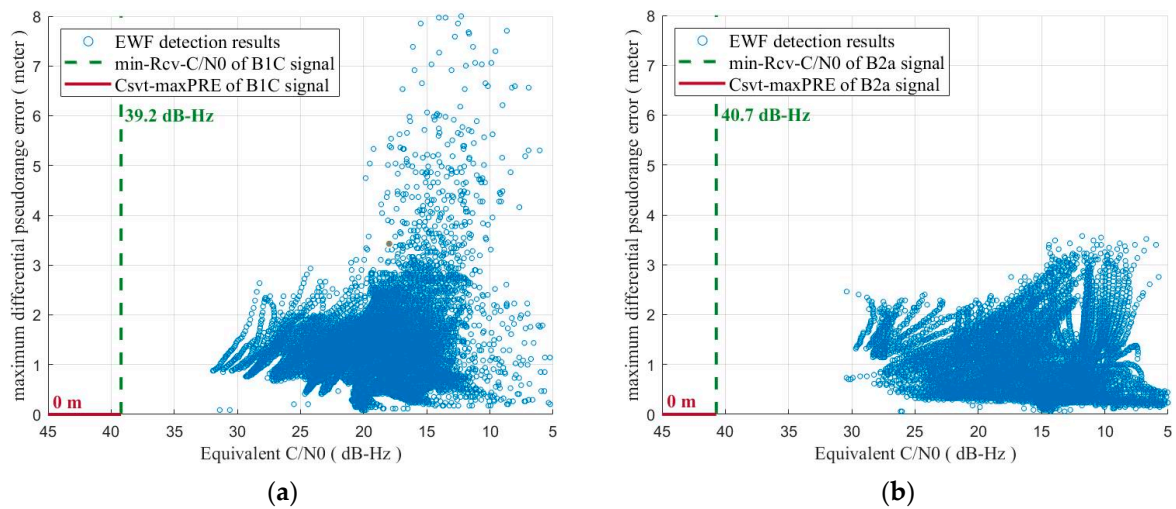


**Figure 3.** Evaluation results of the CDO-based SQM baseline algorithm with a sampling frequency of 72 MHz and bins of 0.025 B1-chips. (a) B1C signal; (b) B2a signal.

Although a satisfactory performance has been achieved by the CDO-based SQM baseline algorithm, it should be noticed that a sampling frequency of 72 MHz introduces implementation complexity to the monitoring receivers. Furthermore, based on the constraint  $F_S \cdot \text{BIN} \leq \text{chip-rate}$  [7], a higher sampling frequency of the RF front-end output with the given chip sectionalization and chip rate of the monitored signal might induce correlations to the samples involved in calculating a CDO value. In addition, the length of code-phase bins is the other key influential factor in SQM design [7]. Therefore, a practicalization of CDO-based SQM algorithm is needed for reducing complexity while providing generality.

#### 4.3. Practicalization of CDO-Based SQM Algorithm

The practicalization of the CDO-based SQM algorithm is on the basis of the design methodology proposed in Reference [7], including the optimizations of bin length to improve overall performance and the iterations of algorithm evaluation to lower sampling frequency, thereby reduce implementation complexity. In this design methodology, an eigen property called critical metric bias (CMB) is defined for the risky group of a signal that is the set of those threat points with maxPREs exceeding the specified MERR with the given TS discretization and receiver configurations. A CMB is expressed by:

$$\text{CMB}_{\text{BIN}, F_S} = \min_{\text{RiskyGroup}} \left\{ \left[ \max_{1 \leq i \leq 848} \left\{ \left| \text{metric}_i^{\text{EWF}} - \text{metric}_i^{\text{nom}} \right| \right\} \right]_{\text{BIN}, F_S} \right\} \quad (21)$$

Specifically, a CMB value, of which the provider within the Risky Group could be deemed the hardest one to detect, is particular to a given configuration of BIN and  $F_S$  [7]. The MERR value will be applied in finding out the CMB values for SQM design. Provided the concept of CMB, the CMB provider of a given configuration of BIN and  $F_S$  will be the determinant of algorithm performance. Thus, an index named figure of merit (FoM) is further defined as:

$$\text{FoM}_{\text{BIN},F_S} = \text{CMB}_{\text{BIN},F_S} / [(K_{\text{ffd}} + K_{\text{md}}) \cdot \sigma_{\text{metric}}] = \frac{\text{CMB}_{\text{BIN},F_S} \cdot F_S \cdot \sqrt{\text{BIN}}}{(K_{\text{ffd}} + K_{\text{md}}) \cdot C_{\text{metric}}} \quad (22)$$

where  $C_{\text{metric}}$  is separated from the expression of  $\sigma_{\text{metric}}$  without factors of BIN and  $F_S$ , e.g.,  $C_{\text{metric}} = BW / I_p / \sqrt{2} \cdot T_{\text{int}} \cdot \text{RER} / 10^{(C/N_0)/20}$  for single-CDO metrics as indicated in Equation (20). Note the differences between Equation (22) and the expression in Reference [7]. The discussions in this paper shall not take the reference-averaging gain into consideration, thus the number of reference stations involved is ignored. The metric-smoothing improvement of 4 dB is absorbed by the  $C/N_0$  in  $C_{\text{metric}}$ , where 39.2 and 40.7 dB-Hz are given for B1C and B2a signals, respectively.

The sectionalization of a chip needs some constraints in order to prevent neither losing necessary information by applying bins too fine, thus causing insufficiency, nor incorporating unnecessary information by utilizing bins too coarse, hence, inducing redundancy, because only 8 CDOs are relevant to the SQM algorithm. Reference [7] gives a method of bin-length selection and performs among GPS L1 C/A, BDS B1C, and BDS B2a signals. The constraints have been detailed and reasoned in Reference [7] and, hence, will not be repeated in this paper for brevity. By applying the constraints in the nominal domain, distortion domain, and rigid domain, given by:

$$\begin{cases} \text{nominal} : [4 \times 68.27\%] \cdot \text{BIN}_{\text{nom}}^{\text{B1C}} < \Delta_1^{\text{nom}} + \Delta_2^{\text{nom}} \\ \text{distorted} : [4 \times 68.27\%] \cdot \text{BIN}_{\text{EWF}}^{\text{B1C}} < \text{chip-rate}/\min\{f_d\} \\ \text{rigid} : 4 \cdot \text{BIN}^{\text{B1C}} < 0.5 \end{cases} \quad (23)$$

the range of bin-length selection for B1C signal is obtained by the intersection as:

$$0.0142 \text{ chips} < \text{BIN}^{\text{B1C}} < 0.0438 \text{ chips} \quad (24)$$

for which the fractional form is expressed as:

$$1/70 \text{ chips} \leq \text{BIN}^{\text{B1C}} \leq 1/23 \text{ chips} \quad (25)$$

where the ratio 68.27% and the featured length  $\Delta_1^{\text{nom}}$  and  $\Delta_2^{\text{nom}}$ , as defined in Reference [7], are measured in the simulated chip rising edge filtered by a 6th-order Butterworth filter, and the range of  $f_d$  that is the frequency of damped oscillation in the 2OS-TM is given in Table 2. The chip period of the B2a signal is one tenth of that of the B1C signal, i.e., 4 bins with a length of 0.025 B1-chips will fulfill a B2 chip since 8 CDOs symmetric about the rising edge are applied. Thus, to the portion of  $0.0142 \text{ chips} < \text{BIN}^{\text{B1C}} < 0.0438 \text{ chips}$  in Equation (24), a B2a code needs more than one consecutive  $-1$  chips followed by the same number of consecutive  $+1$  chips to correspond. Furthermore, accounting for the fact that a chip or the whole of the considered consecutive  $-1$  and/or  $+1$  chips should be sectionalized into integer bins, the range of bin-length selection for B1C signal in Equation (25) could be transformed to that for B2a signal as:

$$\begin{cases} \text{single-chip} : 1/8 \text{ chips} \leq \text{BIN}^{\text{B2a}} \leq 1/4 \text{ chips} \\ \text{dual-chip} : 2/7 \text{ chips} \leq \text{BIN}^{\text{B2a}} \leq 2/5 \text{ chips} \\ \text{triple-chip} : 3/8 \text{ chips} \leq \text{BIN}^{\text{B2a}} \leq 3/7 \text{ chips} \end{cases} \quad (26)$$

where the captions of single-, dual-, and triple-chip indicate the situations of  $(-1,+1)$ ,  $(-1,-1,+1,+1)$ , and  $(-1,-1,-1,+1,+1,+1)$ , respectively. The quad-chip situation is not needed according to Equation (24).

On the other hand, the sampling frequency of RF front-end output also needs some constraints. Given the constraint for bin-length selection in Equation (25), the constraint  $F_S \cdot \text{BIN} \leq \text{chip-rate}$  to prevent correlation among samples in measuring CDOs, the B1C chip rate of 1.023 Mcps, and the Nyquist frequency according to the specified pre-correlation bandwidth of reference receiver in Table 4, the considered range for sampling frequency is from 24 MHz to 72 MHz.

#### 4.3.1. Optimal Bin Length with Equal MERRs

Given the MERR of 3.64 m in Equation (8) for BDS B1C/B2a combinations, the biases of each SF signal will be expressed as  $b_{B1}$  and  $b_{B2}$ , respectively. Assuming that  $|b_{B1}| = |b_{B2}|$ , the maximum allowable  $|b_{B1/B2}|$ , i.e., the MERRs for the individual SF signals in DF applications, shall be given by:

$$\text{MERR}_{\text{DF}}^{\text{B1C/B2a}} = 1.41 \text{ m} \quad (27)$$

Massive simulations are performed across the ranges of BIN and  $F_S$  to obtain the FoM values. Figure 4a,b show the FoM contours of B1C and B2a signals, respectively, with the 1.41-m MERR given in Equation (27). The portions with FoM values not lower than unity indicate satisfactory performance, while the rest need further examination. With any given BIN value, the FoM values are positively correlated with the  $F_S$  values for most of the contours, being consistent with the FoM expression in Equation (23). However, with any given  $F_S$  value, the trends of FoM values are not monotonic about the BIN values. Note that  $\text{CMB}_{\text{BIN},F_S}$  might not be critically identical across the considered range of  $F_S$  but have little impact according to the calculation of CDOs in Equation (12). Thus, the contours in Figure 4 are reduced vertically with the weights corresponding to  $1/F_S$ , e.g., a weight of  $(1/72)/(1/72 + 1/69 + \dots + 1/24) \approx 0.0352$  for a contour value of  $F_S = 72$  MHz with the discretization of 72:–3:24 MHz in simulations.

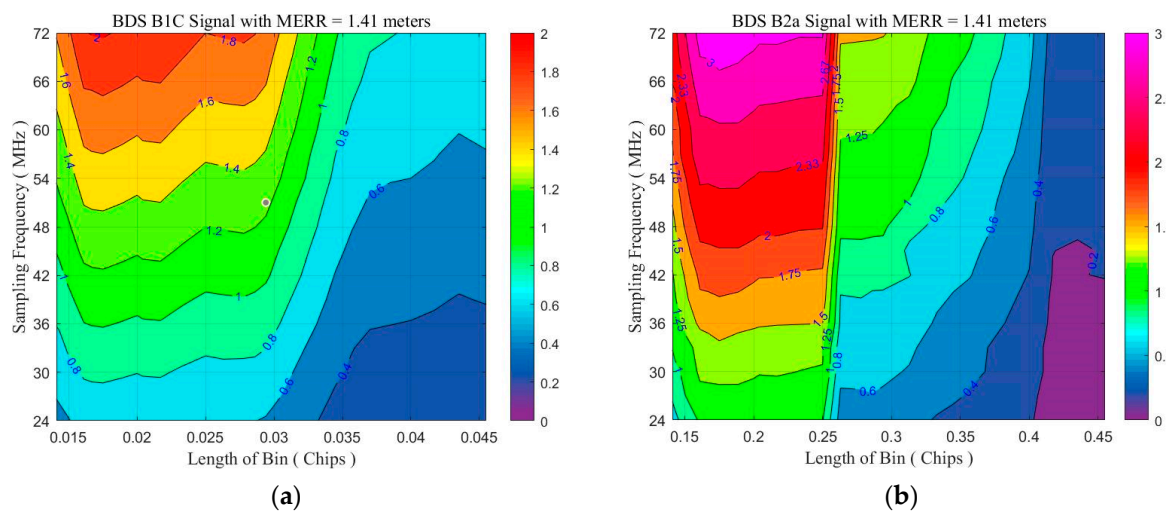


**Figure 4.** Contours of FoM values across the considered ranges of code-phase bin lengths and sampling frequency, with MERR = 1.41 m. (a) B1C signal; (b) B2a signal.

The results of contour reduction are shown in Figure 5. The best performance with the B1C signal could be achieved at the bin-length of  $1/57$  B1-chips. This value is nearer to  $1/6$  B2-chips than to  $1/5$  B2-chips. Correspondingly, the reduced FoM value at  $1/60$  B1-chips for the B1C signal is larger than that at  $1/50$  B1-chip. Moreover, the FoM value of the B2a signal at either  $1/6$  B2-chip or  $1/5$  B2-chips, or even the virtual

1/5.7 B2-chip, is beyond unity with the lowest  $F_S$  of 24 MHz, as shown in Figure 4b. Therefore, the optimal code-phase bin length is temporarily determined as 1/60 B1-chips or 16.292 nanoseconds per bin, being inconsistent with the result in Reference [7] where three representative signals, i.e., GPS L1 C/A, BDS B1C, and BDS B2a, are involved.

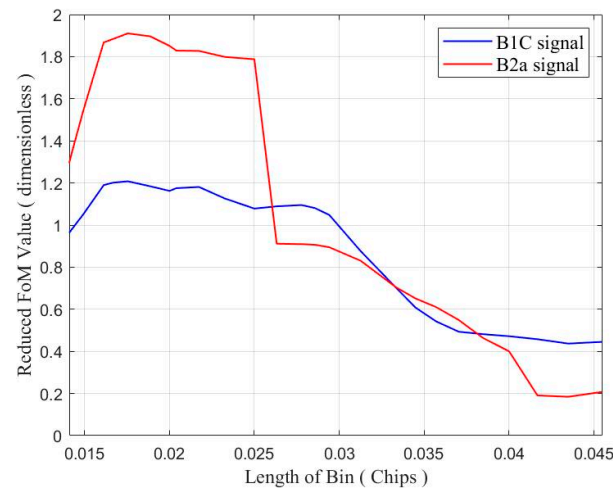


**Figure 5.** Curves of weighed FoM values after contour reduction, with equal MERRs.

Given the temporarily optimal code-phase bin length of 1/60 B1-chips, the considered lowest  $F_S$  of 24 MHz should be evaluated, in order to reduce implementation complexity. The  $C_{svt\_maxPRE}$  values of 1.24 m and 0.59 m, respectively, are obtained, thereby a  $DF\_C_{svt\_maxPRE}$  of 2.90 m corresponding to  $DFREI = 4$  [13] is achieved. Moreover, the performance margins are about 0.5 and 4.3 dB, respectively, i.e., if the preset  $min\_Rcv\_C/N_0$  values of 39.2 and 40.7 dB-Hz were virtually reduced to as low as 38.7 and 36.4 dB-Hz, respectively, the performance of a protection equivalent to DFREI-4 would still sustain.

The configuration with an  $F_S$  of 24 MHz and bin length of 1/60 B1-chips has been evaluated satisfactory under the requirements of DFMC SBAS and practical with low implementation complexity. However, there might still be some optimizations to exploit.

#### 4.3.2. Optimal Bin Length with Unequal MERRs

Since the FoM values of the B2a signal at 1/6, 1/5, and 1/4 B2-chips with 24 MHz are beyond unity as shown in Figure 4b, the MERR for the B2a signal is radicalized as 0 m, as indicated in Figure 3b. Correspondingly, the MERR for the B1C signal is loosened as  $3.64/2.26 \approx 1.61$  m. The new contours are shown in Figure 6.

The contour values in Figure 6a are slightly higher than those in Figure 4a, i.e., +0.0452 in weighted average. Meanwhile, the contour values in Figure 6b are correspondingly lower than those in Figure 4b, i.e.,  $-0.1336$  in weighted average. More specifically for the temporarily optimal code-phase bin length, i.e., 1/60 B1-chip or 1/6 B2-chip, the weighted average differences are +0.0738 and  $-0.4637$ , respectively. While for the adjacent bin length of 1/50 B1-chip or 1/5 B2-chip, the average differences are +0.0898 and  $-0.0866$ , respectively. Thus, this unequal-MERR scheme pays a larger B2a performance loss in exchange for a far smaller B1C performance gain with the temporarily optimal code-phase bin length. However, the situation with a bin length of 1/50 B1-chip or 1/5 B2-chip is nearly balanced. Again, we reduce the contours vertically to get the weighted FoM values, shown in Figure 7.

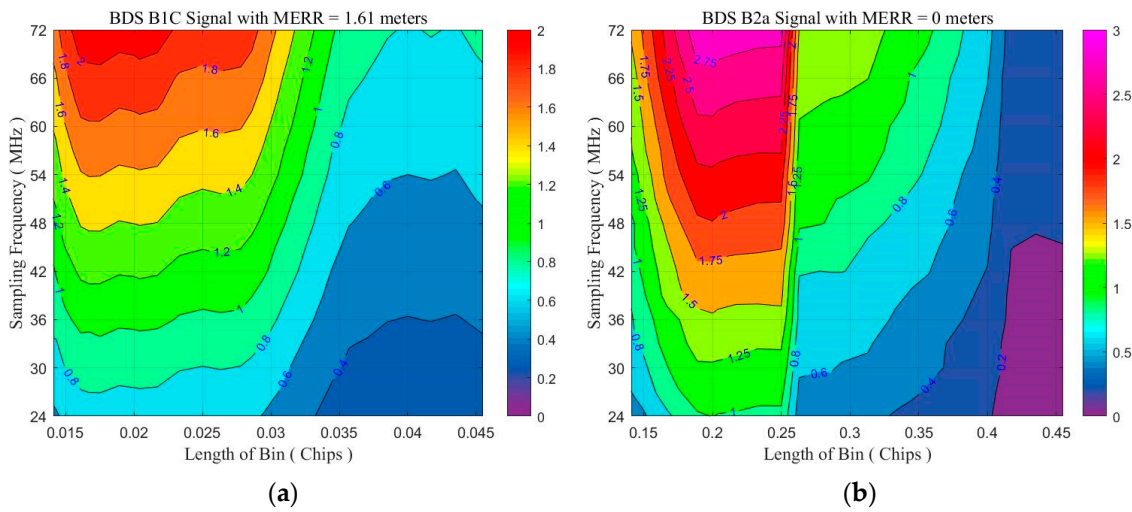


**Figure 6.** Contours of FoM values across the considered ranges of code-phase bin lengths and sampling frequency. (a) B1C signal with MERR = 1.61 m; (b) B2a signal with MERR = 0 m.

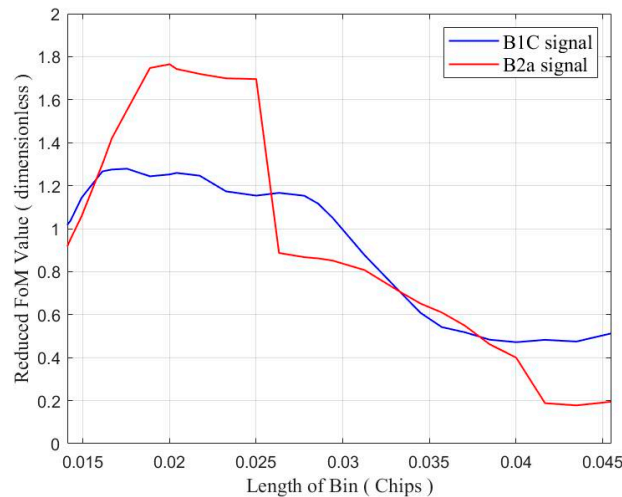


**Figure 7.** Curves of weighed FoM values after contour reduction, with unequal MERRs.

Figure 7 tells that the curve values at 1/60, 1/57, and 1/50 B1-chips are 1.2750, 1.2789, and 1.2522, respectively, for the B1C signal. However, the values for the B2a signal vary significantly. Thus, the optimal code-phase bin length moves forward to 1/50 B1-chips or 19.550 nanoseconds per bin, temporarily. This new temporarily optimal value will be evaluated against the considered lowest  $F_S$  of 24 MHz to find whether the CDO-based SQM algorithm is eligible.

With an  $F_S$  of 24 MHz and bin length of 0.020 B1-chips, the  $DF\_Csvt\_maxPRE$  of BDS B1C/B2a combinations guaranteed by the CDO-based SQM algorithm is calculated as:

$$DF\_Csvt\_maxPRE_{CDO-24-0.020} = 1.32 \times 2.26 \approx 2.98 < 3.64 \text{ m} \tag{28}$$

indicating that a protection equivalent to  $DFREI = 4$  [13] could be provided. The performance margins are about 0.9 and 4.0 dB, respectively.

The performances of the configuration of 1/60-B1-chip bins (cfg-1) and the configuration of 1/50-B1-chip bins (cfg-2) with an  $F_S$  of 24 MHz are compared as follows:

- cfg-1 achieves a lower  $DF\_Csvt\_maxPRE$  value (2.90 m) than cfg-2 does (2.98 m), but the values are comparable;

- cfg-1 provides a total performance margin (4.8 dB) near cfg-2 does (4.9 dB), but the margin for the B1C signal provided by cfg-2 (0.9 dB) is about twice the value provided by cfg-1 (0.5 dB).

Considering the balance between the SQM performance for the two signals and the protection enhancement for the main ranging signal of BDS, i.e., the B1C signal, we decide to choose 1/50-B1-chip or 1/5-B2-chip bins as the optimal value.

To sum up, the CDO-based SQM algorithm with the optimal code-phase sectionalization of 0.020 B1-chips or 0.20 B2-chips identically can provide the required protection that is equivalent to DFREI = 4 with a sampling frequency of the RF front-end output as low as 24 MHz.

#### 4.4. Simplification of CDO-Based SQM Algorithm

As shown in Figures 4 and 6, the contour values corresponding to different BINs vary violently, given a fixed  $F_5$ . The sensitivities of different CDOs to an EWF are closely relevant to the length of bins, due to the modeled fluctuations defined in the 2OS-TM. Reference [7] gives a demonstration to examine the sensitivities of CDOs. In this study, 848 metrics are defined for a CDO-based SQM algorithm in Equation (18). Similarly, the sensitivities of these CDO-based metrics could be examined to simplify the algorithm.

With full metrics, the algorithm could provide DFREI-4 level protection with 0.9- and 4.0-dB performance margins, respectively, as shown in Figure 8. Thus, we examine the sensitivities of metrics with the B1C signal, aiming to combine the detection capabilities of several metrics to hold the 1.61-m MERR limit. Accordingly, the B2a signals applies the same group of metrics as the B1C signal does to keep algorithm consistency.

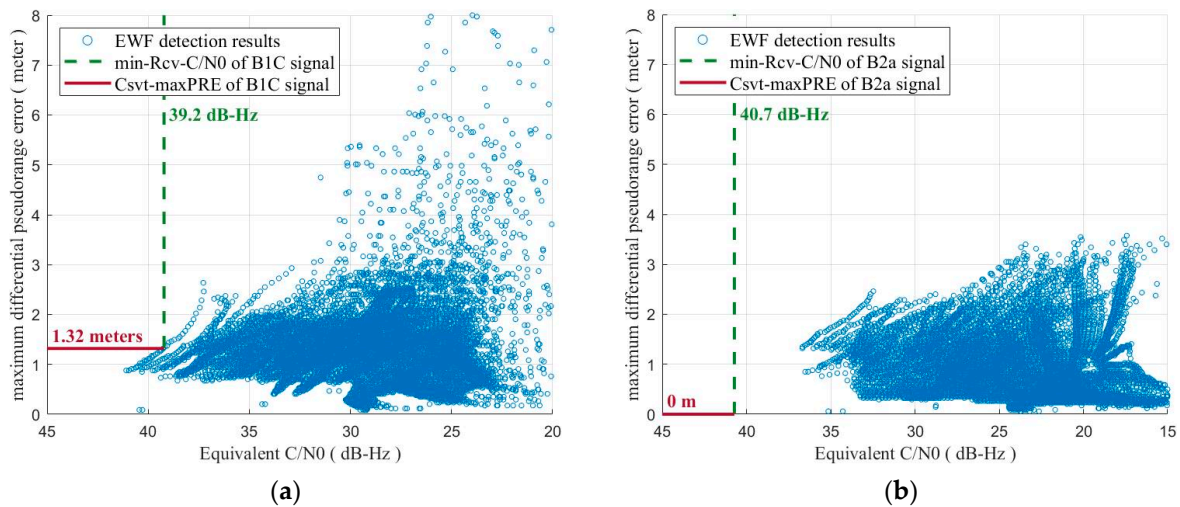


**Figure 8.** Evaluation results of the CDO-based SQM algorithm with a sampling frequency of 24 MHz and bins of 0.020 B1-chips. (a) B1C signal; (b) B2a signal.

(1) Ten metrics are picked out to preserve the performance in Figure 8a, including:

- dual-CDO metrics: (8)  $(CDO_3 - CDO_7)/2$ ,  
(10)  $(CDO_4 - CDO_6)/2$ ,  
(5)  $(CDO_6 - CDO_8)/2$ ;
- triple-CDO metrics: (4)  $(CDO_3 - CDO_5 + CDO_7)/3$ ,  
(3)  $(CDO_4 + CDO_5 - CDO_7)/3$ ,  
(7)  $(CDO_6 + CDO_7 - CDO_8)/3$ ;
- quad-CDO metrics: (2)  $(CDO_3 - CDO_5 + CDO_7 + CDO_8)/4$ ,  
(6)  $(CDO_4 + CDO_5 - CDO_6 - CDO_7)/4$ ,

$$(9) (CDO_4 + CDO_5 - CDO_6 + CDO_8)/4,$$

$$(1) (CDO_4 - CDO_6 - CDO_7 + CDO_8)/4.$$

The indices ahead of the metrics represent the ranks of sensitivities, e.g., (1) means the most sensitive metric while (10) means the least sensitive one among the ten. This group of ten metrics can hold the 0.9-dB performance margin and 1.32-m Csvt\_maxPRE for the B1C signal, while may consume 1.4 dB of the 4-dB performance margin for the B2a signal.

(2) The tenth metric,  $(CDO_4 - CDO_6)/2$ , is removed for another evaluation. This group of nine metrics performs equivalently as the ten-metric group does.

(3) Moreover, the ninth metric,  $(CDO_4 + CDO_5 - CDO_6 + CDO_8)/4$ , is removed for further evaluation. This group of eight metrics consumes 0.4 dB of the 0.9-dB performance margin for the B1C signal.

(4) However, if the eighth metric,  $(CDO_3 - CDO_7)/2$ , is removed, the Csvt\_maxPRE values of B1C and B2a signals would increase to about 3.05 and 0.53 m, respectively, meaning a 6.93-m DF\_Csvt\_maxPRE equivalent to a protection of DFREI = 7 [13].

Therefore, the eight-metric group is the result of algorithm simplification that we suggest for BDS B1C/B2a combinations toward DFMC SBAS. The algorithm is summarized in Table 5. This algorithm is named Chip Domain Signal Quality Monitoring with 8 CDOs in rising-edges (CDSQM8r).

**Table 5.** The CDO-based SQM algorithm for BDS B1C/B2a signals toward DFMC SBAS.

Algorithm Name		CDSQM8r	
Signal		BDS B1C	BDS B2a
Configuration	Location of CDOs (chips)	$\pm 0.01, \pm 0.03, \pm 0.05, \pm 0.07$	$\pm 0.1, \pm 0.3, \pm 0.5, \pm 0.7$
	Sampling Frequency (MHz)	$\geq 24$	
	Integration Period (second)	1	
	Detection Metrics	$(CDO_3 - CDO_7)/2, (CDO_6 - CDO_8)/2,$ $(CDO_3 - CDO_5 + CDO_7)/3, (CDO_4 + CDO_5 - CDO_7)/3,$ $(CDO_6 + CDO_7 - CDO_8)/3,$ $(CDO_3 - CDO_5 + CDO_7 + CDO_8)/4,$ $(CDO_4 + CDO_5 - CDO_6 - CDO_7)/4,$ $(CDO_4 - CDO_6 - CDO_7 + CDO_8)/4$	
	Smoothing Constant (second)	100	
Requirement	Probability of Fault-Free-Detection	$1.5 \times 10^{-7}$ per test	
	Probability of Miss-Detection	$1 \times 10^{-3}$ per test	
	Dual-Frequency User Differential Ranging Error (meter)	3.64 (index 4)	

## 5. Conclusions

BDSBAS is under construction and has formed the initial operational capability by 2022 [3]. In 2025, the DFMC service must be playing a significant role in BDSBAS services toward civil aviation and many other life-safety fields. The integrity monitoring architecture is important for an SBAS in enhancing GNSS integrity, where signal deformation would be the largest source of ranging uncertainty in dual-frequency applications. This paper systematically studies the SQM for BDS B1C/B2a civilian signals and proposes the design methodology for SQM algorithm, which can be seen as a paradigm for the DF civilian signals of any GNSS core constellation under given TM, TS, and performance requirements, which, thus, can easily be extended in the name of DFMC.

The traditional MCO-based and the emerging CDO-based SQM baseline algorithms are fully evaluated and discussed. Moreover, in order to promote overall performance while preserving a lower implementation complexity, a whole design procedure of a CDO-based algorithm is performed, including the operations of practicalization and simplification. In the practicalizing operations, the optimal code-phase bin length is achieved with low sampling frequency of the RF front-end output. While in the simplifying operations, the sensitivity of metrics is examined, hence, the number of necessary metrics are sharply reduced for computational complexity. Finally, an algorithm named CDSQM8r is proposed for BDS B1C/B2a signals.

The CDSQM8r algorithm proposed in this paper could be considered as an effective candidate of DF SQM in the developing BDSBAS and other new generation DFMC SBASs for BDS DF civilian signals. Furthermore, once provided the standard 2OS-TM, the specific TSs, and the requirements equivalent to that of CAT-I PA in civil aviation, other algorithms might be worked out for the combinations of GPS L1C/A/L5-Q, GLONASS L1OCd/L3OC, and Galileo E1-C/E5a-Q. After checking the compatibility and interoperability of these potential algorithms, the generic CDO-based SQM algorithm towards DFMC SBAS would be reached.

**Author Contributions:** Conceptualization, X.W. and X.C.; Funding acquisition, M.L.; Investigation, X.W.; Methodology, X.W.; Project administration, M.L.; Software, X.W.; Supervision, M.L.; Writing—original draft, X.W.; Writing—review & editing, X.W., X.C., G.L. and M.L. All authors have read and agreed to the published version of the manuscript.

**Funding:** This research was funded by the National Key R&D Program of China under Grant No. 2021YFA0716603.

**Data Availability Statement:** Not applicable. No publicly archived dataset is used in this study. All the data relative to the study is generated by local simulations, including the anomalous signals generation according to the Threat Model, the filter design according to the specified reference receiver configuration, the SQM detections and algorithm evaluations according to the proposed methodology, etc. Scholars and researchers interested in the field of study would simply generate the data in accordance with the formulations.

**Acknowledgments:** The authors would like to thank all the editors and reviewers for their patience, professionalism, and constructive comments.

**Conflicts of Interest:** The authors declare no conflict of interest.

## Appendix A

Given the integration period  $T$ , the noise power  $\sigma^2 = 1$ , and the considered carrier-to-noise ratio  $C/N_0$ , the signal amplitude is calculated as:

$$A = \sqrt{2 \cdot C} = \sqrt{2 \cdot N_0 \cdot 10^{\frac{C/N_0}{10}}} = \sqrt{2 \cdot \frac{4 \cdot \sigma^2}{T} \cdot 10^{\frac{C/N_0}{10}}} = \sqrt{\frac{8}{T}} \cdot 10^{\frac{C/N_0}{20}} \quad (\text{A1})$$

Then, the in-phase component of correlator value of correlator  $x$  is written as:

$$I_x = MR_x A \cdot \frac{T}{2} + \sum_{j=1}^M n_{0,j} = MKR_x + \sum_{j=1}^M n_{x,j} \quad (\text{A2})$$

where  $M = 1/T$  is the number of integrations in one second,  $K = A \cdot T/2 = \sqrt{2T} \cdot 10^{(C/N_0)/20}$  is deemed constant,  $R_x$  is the ideal correlator value at the location  $x$ , and  $n_{x,j} \sim \mathcal{N}(0, 1)$  is the noise term of the  $j$ -th integration. Thus,  $MK^2 = 2 \times 10^{(C/N_0)/10}$ .

Consider simple-ratio metrics with the definition  $\text{metric}_{\text{simple-ratio}} \triangleq I_x / I_p$ . By applying 1st-order Taylor expansion, the expectation and variation of a simple-ratio metric can be derived as:

$$E\left(\frac{I_x}{I_p}\right) = E\left(\frac{MKR_x + \sum_{j=1}^M n_{x,j}}{MKR_0 + \sum_{j=1}^M n_{0,j}}\right) \stackrel{t=\frac{\sum_{j=1}^M n_{0,j}}{MKR_0}}{=} \frac{1}{MK} E\left(\frac{MKR_x + \sum_{j=1}^M n_{x,j}}{1+t}\right) \approx \frac{1}{MK} E\left(\left(MKR_x + \sum_{j=1}^M n_{x,j}\right) \left(\sum_{n=0}^{\infty} (-1)^n t^n\right)\right) \triangleq \frac{1}{MK} E(XY) \tag{A3}$$

$$\begin{aligned} \text{var}\left(\frac{I_x}{I_p}\right) &= \text{var}\left(\frac{MKR_x + \sum_{j=1}^M n_{x,j}}{MKR_0 + \sum_{j=1}^M n_{0,j}}\right) \stackrel{t=\frac{\sum_{j=1}^M n_{0,j}}{MKR_0}}{=} \frac{1}{M^2K^2} \text{var}\left(\frac{MKR_x + \sum_{j=1}^M n_{x,j}}{1+t}\right) \\ &\approx \frac{1}{M^2K^2} \text{var}\left(\left(MKR_x + \sum_{j=1}^M n_{x,j}\right) \left(\sum_{n=0}^{\infty} (-1)^n t^n\right)\right) \triangleq \frac{1}{M^2K^2} \text{var}(XY) \end{aligned} \tag{A4}$$

Note that  $R_0 = 1$  theoretically. Since

$$XY = \left(MKR_x + \sum_{j=1}^M n_{x,j}\right) \left(1 - \frac{1}{MKR_0} \sum_{j=1}^M n_{0,j}\right) = MKR_x + \sum_{j=1}^M n_{x,j} - R_x \sum_{k=1}^M n_{0,k} - \frac{1}{MK} \sum_{j=1}^M n_{x,j} \sum_{k=1}^M n_{0,k} \tag{A5}$$

the expectation and variation of  $XY$  are given by:

$$E(XY) = MKR_x + 0 - 0 - \frac{1}{MK} E\left(\sum_{j=1}^M n_{x,j} \sum_{k=1}^M n_{0,k}\right) = MKR_x - \frac{1}{MK} \sum_{1 \leq j=k \leq M} E(n_{x,j} n_{0,k}) = MKR_x - \frac{R_x}{K} = MKR_x \left(1 - \frac{1}{MK^2}\right) \tag{A6}$$

$$\begin{aligned} \text{var}(XY) &= E(X^2Y^2) - (E(XY))^2 \\ &= E\left(\left(MKR_x + \sum_{j=1}^M n_{x,j} - R_x \sum_{k=1}^M n_{0,k} - \frac{1}{MK} \sum_{j=1}^M n_{x,j} \sum_{k=1}^M n_{0,k}\right)^2\right) - \left(MKR_x \left(1 - \frac{1}{MK^2}\right)\right)^2 \\ &= (MKR_x)^2 + E\left(\left(\sum_{j=1}^M n_{x,j}\right)^2\right) + R_x^2 E\left(\left(\sum_{k=1}^M n_{0,k}\right)^2\right) + \frac{1}{M^2K^2} E\left(\left(\sum_{j=1}^M n_{x,j} \sum_{k=1}^M n_{0,k}\right)^2\right) + 2MKR_x E\left(\sum_{j=1}^M n_{x,j}\right) \\ &\quad - 2MKR_x^2 E\left(\sum_{k=1}^M n_{0,k}\right) - 2R_x E\left(\sum_{j=1}^M n_{x,j} \sum_{k=1}^M n_{0,k}\right) - 2R_x E\left(\sum_{j=1}^M n_{x,j} \sum_{k=1}^M n_{0,k}\right) - \frac{2}{MK} E\left(\sum_{j=1}^M n_{x,j} \sum_{j=1}^M n_{x,j} \sum_{k=1}^M n_{0,k}\right) \\ &\quad + \frac{2R_x}{MK} E\left(\sum_{k=1}^M n_{0,k} \sum_{j=1}^M n_{x,j} \sum_{k=1}^M n_{0,k}\right) - \left(MKR_x \left(1 - \frac{1}{MK^2}\right)\right)^2 \\ &= (MKR_x)^2 + M + MR_x^2 + \frac{1}{M^2K^2} E\left(\left(\sum_{j=1}^M n_{x,j} \sum_{k=1}^M n_{0,k}\right)^2\right) + 0 - 0 - 2MR_x^2 - 2MR_x^2 \\ &\quad - \frac{2}{MK} E\left(\sum_{j=1}^M n_{x,j} \sum_{j=1}^M n_{x,j} \sum_{k=1}^M n_{0,k}\right) + \frac{2R_x}{MK} E\left(\sum_{k=1}^M n_{0,k} \sum_{j=1}^M n_{x,j} \sum_{k=1}^M n_{0,k}\right) - \left(MKR_x \left(1 - \frac{1}{MK^2}\right)\right)^2 \\ &= M(1 - R_x^2) - \frac{R_x^2}{K^2} + \frac{1}{M^2K^2} E\left(\left(\sum_{j=1}^M n_{x,j} \sum_{k=1}^M n_{0,k}\right)^2\right) - \frac{2}{MK} E\left(\sum_{j=1}^M n_{x,j} \sum_{j=1}^M n_{x,j} \sum_{k=1}^M n_{0,k}\right) + \frac{2R_x}{MK} E\left(\sum_{k=1}^M n_{0,k} \sum_{j=1}^M n_{x,j} \sum_{k=1}^M n_{0,k}\right) \end{aligned} \tag{A7}$$

By ignoring the latter three higher order terms in Equation (A7) and substituting the result into Equations (A3) and (A4), respectively, the expectation and variation of a simple-ratio metric are derived as:

$$E\left(\frac{I_x}{I_p}\right) \approx \frac{1}{MK} \cdot MKR_x \left(1 - \frac{1}{MK^2}\right) = R_x \left(1 - \frac{1}{MK^2}\right) = \begin{cases} (1 - 3|x|) \left(1 - \frac{1}{MK^2}\right) & \text{B1C}(-0.5 \leq x \leq +0.5) \\ (1 - |x|) \left(1 - \frac{1}{MK^2}\right) & \text{B2a}(-1.0 \leq x \leq +1.0) \end{cases} \tag{A8}$$

$$\text{var}\left(\frac{I_x}{I_p}\right) \approx \frac{1}{M^2K^2} \cdot \left(M(1 - R_x^2) - \frac{R_x^2}{K^2}\right) = \frac{1 - R_x^2}{MK^2} - \frac{R_x^2}{(MK^2)^2} = \begin{cases} \frac{6|x| - 9|x|^2}{MK^2} - \left(\frac{1 - 3|x|}{MK^2}\right)^2 & \text{B1C}(-0.5 \leq x \leq +0.5) \\ \frac{2|x| - |x|^2}{MK^2} - \left(\frac{1 - |x|}{MK^2}\right)^2 & \text{B2a}(-1.0 \leq x \leq +1.0) \end{cases} \tag{A9}$$

Consider diff- and sum-ratio metrics with the definition  $\text{metric}_{\text{diff-ratio}} \triangleq (I_{-x} - I_x)/I_p$  and  $\text{metric}_{\text{sum-ratio}} \triangleq (I_{-x} + I_x)/I_p$ . The covariance between  $I_x/I_p$  and  $I_{-x}/I_p$  should be checked first. The expectation of the product of  $I_x/I_p$  and  $I_{-x}/I_p$  is given as:

$$\begin{aligned}
 E\left(\frac{I_x}{I_p} \cdot \frac{I_{-x}}{I_p}\right) &= E\left(\frac{MKR_x + \sum_{j=1}^M n_{x,j}}{MKR_0 + \sum_{j=1}^M n_{0,j}} \cdot \frac{MKR_{-x} + \sum_{j=1}^M n_{-x,j}}{MKR_0 + \sum_{j=1}^M n_{0,j}}\right) \stackrel{t=1}{=} \frac{\sum_{j=1}^M n_{0,j}}{MKR_0} \frac{1}{M^2 K^2} E\left(\frac{MKR_x + \sum_{j=1}^M n_{x,j}}{1+t} \cdot \frac{MKR_{-x} + \sum_{j=1}^M n_{-x,j}}{1+t}\right) \\
 &\approx \frac{1}{M^2 K^2} E\left(\left(MKR_x + \sum_{j=1}^M n_{x,j}\right) \left(1 - \frac{1}{MK} \sum_{j=1}^M n_{0,j}\right) \left(MKR_{-x} + \sum_{j=1}^M n_{-x,j}\right) \left(1 - \frac{1}{MK} \sum_{j=1}^M n_{0,j}\right)\right) \\
 &= \frac{1}{M^2 K^2} E\left(\left(MKR_x - R_x \sum_{k=1}^M n_{0,k} + \sum_{j=1}^M n_{x,j} - \frac{1}{MK} \sum_{j=1}^M n_{x,j} \sum_{k=1}^M n_{0,k}\right) \left(MKR_{-x} - R_x \sum_{k=1}^M n_{0,k} + \sum_{j=1}^M n_{-x,j} - \frac{1}{MK} \sum_{j=1}^M n_{-x,j} \sum_{k=1}^M n_{0,k}\right)\right) \\
 &\approx \frac{1}{M^2 K^2} \left(M^2 K^2 R_x^2 - MKR_x^2 E\left(\sum_{k=1}^M n_{0,k}\right) + MKR_x E\left(\sum_{j=1}^M n_{-x,j}\right) - R_x E\left(\sum_{j=1}^M n_{-x,j} \sum_{k=1}^M n_{0,k}\right) - MKR_x^2 E\left(\sum_{k=1}^M n_{0,k}\right) + R_x^2 E\left(\sum_{k=1}^M n_{0,k} \sum_{k=1}^M n_{0,k}\right)\right) \\
 &\quad - R_x E\left(\sum_{k=1}^M n_{0,k} \sum_{j=1}^M n_{-x,j}\right) + MKR_x E\left(\sum_{j=1}^M n_{x,j}\right) - R_x E\left(\sum_{j=1}^M n_{x,j} \sum_{k=1}^M n_{0,k}\right) + E\left(\sum_{j=1}^M n_{x,j} \sum_{j=1}^M n_{-x,j}\right) - R_x E\left(\sum_{j=1}^M n_{x,j} \sum_{k=1}^M n_{0,k}\right) \\
 &= \frac{1}{M^2 K^2} \cdot (M^2 K^2 R_x^2 - 0 + 0 - MR_x^2 - 0 + MR_x^2 - MR_x^2 + 0 - MR_x^2 + MR_{2x} - MR_x^2) \\
 &= R_x^2 + \frac{R_{2x} - 3R_x^2}{MK^2}
 \end{aligned} \tag{A10}$$

Note that  $R_x = R_{-x}$  theoretically. Then, the covariance is given by:

$$\begin{aligned}
 \text{cov}\left(\frac{I_x}{I_p}, \frac{I_{-x}}{I_p}\right) &= E\left(\frac{I_x}{I_p} \cdot \frac{I_{-x}}{I_p}\right) - E\left(\frac{I_x}{I_p}\right)E\left(\frac{I_{-x}}{I_p}\right) = R_x^2 + \frac{R_{2x} - 3R_x^2}{MK^2} - R_x \left(1 - \frac{1}{MK^2}\right) \cdot R_{-x} \left(1 - \frac{1}{MK^2}\right) \\
 &= \frac{R_{2x} - R_x^2}{MK^2} - \frac{R_x^2}{(MK^2)^2}
 \end{aligned} \tag{A11}$$

The variances of a diff- and a sum-ratio metrics are expressed by:

$$\begin{aligned}
 \text{var}\left(\frac{I_x \mp I_{-x}}{I_p}\right) &= \text{var}\left(\frac{I_x}{I_p}\right) + \text{var}\left(\frac{I_{-x}}{I_p}\right) \mp 2 \cdot \text{cov}\left(\frac{I_x}{I_p}, \frac{I_{-x}}{I_p}\right) = 2 \cdot \left(\frac{1 - R_x^2}{MK^2} - \frac{R_x^2}{(MK^2)^2}\right) \mp 2 \cdot \left(\frac{R_{2x} - R_x^2}{MK^2} - \frac{R_x^2}{(MK^2)^2}\right) \\
 &= \begin{cases} \text{diff} : \frac{2 - 2R_{2x}}{MK^2} \\ \text{sum} : \frac{2 - 4R_x^2 + 2R_{2x}}{MK^2} - \frac{4R_x^2}{(MK^2)^2} \end{cases} = \begin{cases} \text{diff} : \begin{cases} \frac{12|x|}{MK^2} & \text{B1C}(-0.25 \leq x \leq +0.25) \\ \frac{4|x|}{MK^2} & \text{B2a}(-0.5 \leq x \leq +0.5) \\ \frac{2}{MK^2} & \text{B2a}(0.5 < |x| \leq 1.0) \end{cases} \\ \text{sum} : \begin{cases} \frac{12|x| - 36|x|^2}{MK^2} - \frac{4 \cdot (1 - 3|x|)^2}{(MK^2)^2} & \text{B1C}(-0.25 \leq x \leq +0.25) \\ \frac{4|x| - 4|x|^2}{MK^2} - \frac{4 \cdot (1 - |x|)^2}{(MK^2)^2} & \text{B2a}(-0.5 \leq x \leq +0.5) \\ \frac{2 - 4 \cdot (1 - |x|)^2}{MK^2} - \frac{4 \cdot (1 - |x|)^2}{(MK^2)^2} & \text{B2a}(0.5 < |x| \leq 1.0) \end{cases} \end{cases} \tag{A12}
 \end{aligned}$$

Figure A1 shows the comparisons between the MDE values from theoretical calculations based on the above derivations and those from Monte Carlo simulations for B1C and B2a signals, respectively.

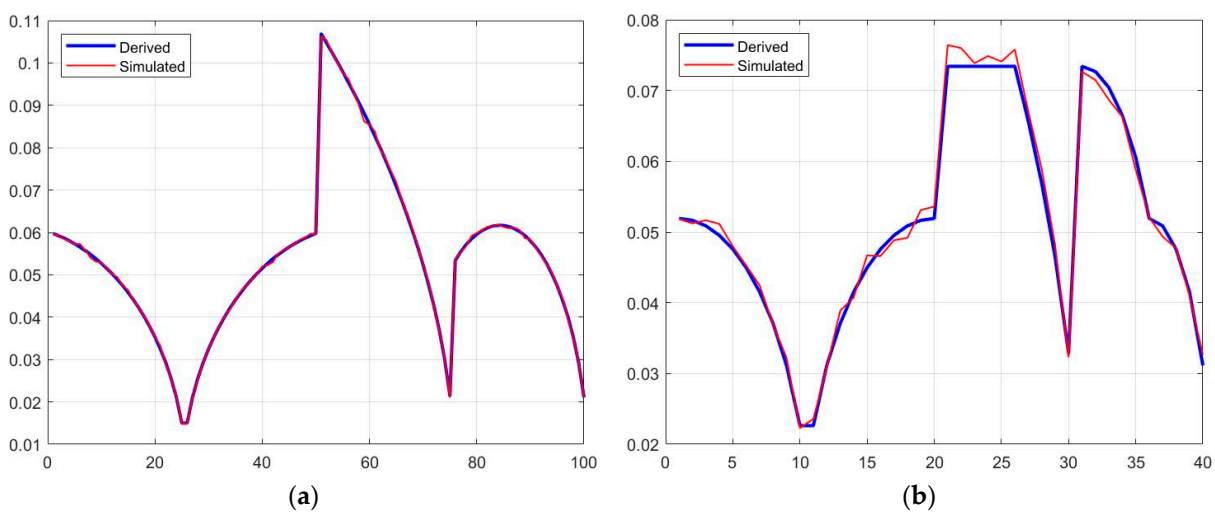


Figure A1. Comparisons between MDE values from theoretical derivations and Monte Carlo simulations. (a) B1C signal; (b) B2a signal.

## References

1. International Civil Aviation Organization. Aeronautical Telecommunications (Annex 10 to the Convention on International Civil Aviation): Radio Navigation Aids (Volume I). In *International Standards and Recommended Practices*, 7th ed.; International Civil Aviation Organization: Montreal, QC, Canada, 2018.
2. Enge, P.; Walter, T.; Pullen, S.; Kee, C.; Chao, Y.-C.; Tsai, Y.-J. Wide area augmentation of the Global Positioning System. *Proc. IEEE* **1996**, *84*, 1063–1088. [[CrossRef](#)]
3. Gao, W.; Cao, Y.; Liu, C.; Lu, J.; Shao, B.; Xiong, S.; Su, C. Construction Progress and Aviation Flight Test of BDSBAS. *Remote Sens.* **2022**, *14*, 1218. [[CrossRef](#)]
4. Liu, C.; Gao, W.G.; Shao, B.; Lu, J.; Wang, W.; Chen, Y.; Su, C.G.; Xiong, S.; Ding, Q. Development of BeiDou Satellite-Based Augmentation System. *Navigation* **2021**, *68*, 405–417. [[CrossRef](#)]
5. Zheng, S.; Gao, M.; Huang, Z.; Jin, X.; Li, K. Satellite integrity monitoring for satellite-based augmentation system: An improved covariance-based method. *Satell. Navig.* **2022**, *3*, 9. [[CrossRef](#)]
6. Phelts, R.E. Multi-correlator Techniques for Robust Mitigation of Threats to GPS Signal Quality. Ph.D. Thesis, Stanford University, Stanford, CA, USA, 2001. Available online: <http://web.stanford.edu/group/scpnt/gpslab/pubs/theses/EricPheltsThesis01.pdf> (accessed on 13 January 2020).
7. Wang, X.; Cui, X.; Liu, G.; Wei, K.; Lu, M. Signal Quality Monitoring Based on Chip Domain Observables: Theory, Design, and Implementation. *Navigation* **2022**, *69*, navi.543. [[CrossRef](#)]
8. Shallberg, K.W.; Ericson, S.D.; Phelts, R.E.; Walter, T.; Kovach, K.; Altshuler, E. Catalog and Description of GPS and WAAS L1 C/A Signal Deformation Events. In Proceedings of the ION ITM 2017, Institute of Navigation, Monterey, CA, USA, 30 January–2 February 2017; pp. 508–520. [[CrossRef](#)]
9. Walter, T.; Shallberg, K.; Altshuler, E.; Wanner, W.; Harris, C.; Stimmler, R. WAAS at 15. *Navigation* **2018**, *65*, 581–600. [[CrossRef](#)]
10. Phelts, R.E.; Walter, T.; Enge, P. Toward Real-Time SQM for WAAS: Improved Detection Techniques. In Proceedings of the ION GPS/GNSS 2003, Institute of Navigation, Portland, OR, USA, 9–12 September 2003; pp. 2739–2749. Available online: <https://www.ion.org/publications/abstract.cfm?articleID=5462> (accessed on 13 June 2020).
11. Pagot, J.-B.; Julien, O.; Thevenon, P.; Fernandez, F.A.; Cabantous, M. Signal Quality Monitoring for New GNSS Signals. *Navigation* **2018**, *65*, 83–97. [[CrossRef](#)]
12. Walter, T.; Blanch, J.; Phelts, R.E.; Enge, P. Evolving WAAS to Serve L1/L5 Users. *Navigation* **2012**, *59*, 317–327. [[CrossRef](#)]
13. Phelts, R.E.; Wong, G.; Walter, T.; Enge, P. Signal Deformation Monitoring for Dual-Frequency WAAS. In Proceedings of the ION ITM 2013, Institute of Navigation, San Diego, CA, USA, 27–29 January 2013; pp. 93–106. Available online: <https://www.ion.org/publications/abstract.cfm?articleID=10817> (accessed on 13 June 2020).
14. Fenton, P.C.; Jones, J. The Theory and Performance of NovAtel Inc.’s Vision Correlator. In Proceedings of the ION GNSS 2005, Institute of Navigation, Long Beach, CA, USA, 13–16 September 2005; pp. 2178–2186.
15. Weill, L.R. Theory and Applications of Signal Compression in GNSS Receivers. In Proceedings of the ION GNSS 2007, Institute of Navigation, Fort Worth, TX, USA, 25–28 September 2007; pp. 708–719.
16. Wang, C.; Wang, X.; Cui, X.; Liu, G.; Lu, M. Efficient chip-shape correlator implementation on a GPU-based real-time GNSS SDR receiver. *GPS Solut.* **2022**, *26*, 143. [[CrossRef](#)]
17. Thevenon, P.; Pagot, J.-B.; Julien, O.; Tessier, Q. Processing Technique and Performance of the Observation of Evil Waveform in the Chip Domain. In Proceedings of the IEEE NAVITEC 2014, ESA, Noordwijk, The Netherlands, 3–5 December 2014; Available online: <https://hal-enac.archives-ouvertes.fr/hal-01094193> (accessed on 3 July 2020).
18. Pagot, J.-B.; Thevenon, P.; Julien, O.; Gregoire, Y.; Fernández, F.A.; Maillard, D. Estimation of GNSS Signals’ Nominal Distortions from Correlation and Chip Domain. In Proceedings of the ION ITM 2015, Institute of Navigation, Dana Point, CA, USA, 26–28 January 2015; pp. 415–427. Available online: <https://www.ion.org/publications/abstract.cfm?articleID=12640> (accessed on 22 September 2020).
19. Li, R.D.; Tang, X.M.; Ou, G. GNSS Signal Quality Analysis Technique Based on Chip Measurement. In Proceedings of the IEEE ITOEC 2017, Chongqing, China, 3–5 October 2017; pp. 470–475. [[CrossRef](#)]
20. Wang, X.; Gao, Y.; Cui, X.W.; Liu, G.; Lu, M.Q. A Signal Quality Monitoring Algorithm Based on Chip Domain Observables for BDS B1C signal. In Proceedings of the ION ITM 2021, Institute of Navigation, Virtual, 25–28 January 2021; pp. 149–161. [[CrossRef](#)]
21. Liu, C.; Cao, Y.-L.; Zhang, G.; Gao, W.-G.; Chen, J.; Lu, J.; Liu, C.-H.; Zhao, H.-T. Design and Performance Analysis of BDS-3 Integrity Concept. *Remote Sens.* **2021**, *13*, 2860. [[CrossRef](#)]
22. Chen, L.; Gao, W.G.; Hu, Z.G.; Cao, Y.L.; Pei, L.; Liu, C.; Zhou, W.; Liu, X.Z.; Chen, L.; Yang, R.H. BDS-3 Integrity Risk Modeling and Probability Evaluation. *Remote Sens.* **2022**, *14*, 944. [[CrossRef](#)]
23. International Civil Aviation Organization. *DFMC SBAS SARPs—Part B, Version 2.0. NSP, DS2/WP/3 v2.0*; International Civil Aviation Organization: Montreal, QC, Canada, 2018.
24. Lu, M.; Li, W.; Yao, Z.; Cui, X. Overview of BDS III new signals. *Navigation* **2019**, *66*, 19–35. [[CrossRef](#)]
25. China Satellite Navigation Office. BeiDou Navigation Satellite System Signal in Space Interface Control Document, Open Service Signal B1C (Version 1.0). December 2017. Available online: <http://www.beidou.gov.cn/xt/gfzx/201712/P020171226741342013031.pdf> (accessed on 9 October 2020).

26. China Satellite Navigation Office. BeiDou Navigation Satellite System Signal in Space Interface Control Document, Open Service Signal B2a (Version 1.0). December 2017. Available online: <http://www.beidou.gov.cn/xt/gfxz/201712/P020171226742357364174.pdf> (accessed on 9 October 2020).
27. Cui, X.W. Applicability Analysis of the Filter Gain Roll-off in DFMC SBAS Receiver Design Constraints for BDS B1C and B2a Signals. In Proceedings of the ICAO, NSP, JWGs/6-WP/24, Virtual, 5 June 2020.
28. Shloss, P.; Phelts, R.E.; Walter, T.; Enge, P. A Simple Method of Signal Quality Monitoring for WAAS LNAV/VNAV. In Proceedings of the ION GPS 2002, Institute of Navigation, Portland, OR, USA, 24–27 September 2002; pp. 800–808. Available online: <https://www.ion.org/publications/abstract.cfm?articleID=2083> (accessed on 2 May 2020).
29. Shao, B.; Ding, Q.; Wu, X.B. Estimation method of SBAS dual-frequency range error integrity parameter. *Satell. Navig.* **2020**, *1*, 9. [[CrossRef](#)]
30. Wang, X.; Cui, X.W.; Wei, K.F.; Liu, G.; Gao, Y.; Lu, M.Q. Signal Quality Monitoring Algorithms of DFMC SBAS for Dual-Frequency Civil Signals of BDS. In Proceedings of the CSNC 2021, Nanchang, China, 26–28 May 2021; Lecture Notes in Electrical Engineering Volume 773. Springer: Berlin/Heidelberg, Germany, 2021; pp. 75–91. [[CrossRef](#)]
31. Wang, X.; Cui, X.W.; Liu, G.; Tian, Z.Y.; Lu, M.Q. Performance Evaluation of Two Kinds of Error Correlation Function Generation Methods for Signal Deformation Monitoring. In Proceedings of the ION ITM 2022, Institute of Navigation, Long Beach, CA, USA, 25–27 January 2022; pp. 389–400. [[CrossRef](#)]
32. NovAtel. *GNSS-750 Antenna Guide, OM-20000120, Rev 5*; NovAtel Inc.: Calgary, AB, Canada, 2012.
33. Wang, X.; Cui, X.W.; Liu, G.; Qi, H.T.; Lu, M.Q. Necessity and Modeling of the Satellite-induced Elevation-dependent Signal Anomalies for SBAS Integrity Monitoring. In Proceedings of the ION GNSS+ 2022, Institute of Navigation, Denver, CO, USA, 19–23 September 2022; pp. 2777–2789. [[CrossRef](#)]

**Disclaimer/Publisher’s Note:** The statements, opinions and data contained in all publications are solely those of the individual author(s) and contributor(s) and not of MDPI and/or the editor(s). MDPI and/or the editor(s) disclaim responsibility for any injury to people or property resulting from any ideas, methods, instructions or products referred to in the content.